Adsorption of Whey Protein and Sodium Caseinate on Colloidal Cr_2O_3 as a Model for the Prefouling of Steel

Bram Bemelmans

Master's thesis, Nanomaterials Science program, Utrecht University

Date: *29-1-2024*

Van 't Hoff laboratory for Physical and Colloid Chemistry, Debye Institute for Nanomaterials Science, Utrecht University

Supervisors: Dr. R. Hans Tromp (*NIZO food research*), Dr. Ben H. Erné (*UU*)

Abstract

The adsorption of whey protein (β-lactoglobulin/α-lactalbumin) and NaCas ($\alpha_{s1}/\alpha_{s2}/\beta/\kappa$-caseins) onto colloidal Cr_2O_3 was examined at 20 °C as a model for the prefouling of steel . The role of electrostatic interactions in formation of a monolayer of adsorbed protein was studied by characterizing the adsorption as function of pH. From zeta potential measurements NaCas and whey proteins were found to have their isoelectric point around pH 5 and colloidal Cr_2O_3 an isoelectric point of pH 3, similar to stainless steel. Expecting maximum adsorption in a pH range where surface charges have opposite signs, we assessed whey protein and NaCas adsorption onto Cr_2O_3 in the pH range 3 to 7. Colloidal stability analysis indicated protein adsorption through its stabilizing effect on the Cr_2O_3 dispersions. Stabilization by adsorbed NaCas was not found to be pH dependent Whey proteins were found to stabilize Cr_2O_3 marginally less at low pH than at neutral pH. Similarly, adsorption isotherms constructed via UV-Vis spectroscopy, revealed that adsorption of NaCas onto Cr_2O_3 was pH-independent and whey protein adsorbed less at low pH than at neutral pH. From these findings, we conclude that electrostatic interactions are not the primary factor in monolayer adsorption of milk proteins. These findings contribute to the understanding required for the development of better strategies to mitigate protein fouling in the food industry.

Contents

Introduction

The unwanted adsorption of proteins onto solid surfaces is a persistent problem in the food industry. It is an almost unavoidable problem when working with proteins in solution. Therefore for decades, the phenomena that dictate the adsorption of proteins onto solid surfaces have been actively researched. In industry, this issue is called fouling and is present nearly everywhere where solutions containing proteins are processed [1]. Milk is a prime candidate for fouling because it is a protein rich fluid that has to be heat treated for consumption, a process called pasteurization. During the heat treatment, fouling occurs, and layers of protein and salts adhere irreversibly on the steel surface used in heat diffusers[2]. These adsorbed fouling layers must be periodically removed to keep a dairy processing plant functional because they reduce the flow in the steel pipes and provide a substrate for the growth of microbial contaminates[3]. The cleaning of these fouling layers is a labor and chemically intensive process[4]. The economic impact of fouling cannot be underestimated as the cleaning of fouling accounts for 15% of production time [5] and up to 80 % production cost are attributed to cleaning and removal of fouling [6]. In the dairy industry, billions of euros are lost each year and it has a significant impact on the environment. Furthermore, in recent years non-dairy alternatives have gained a large part of the global food market [7]. This has happened in part because it has become clear that the protein transition, the shift away from animal proteins toward plant-based proteins, is an unmissable part in the reduction in our carbon footprint[8]. Plant-based proteins encounter the same fouling problem as traditional dairy products [9], [10], [11]. Therefore, it is now more than ever relevant to gain more understanding of fouling.

As fouling is a persistent issue in the food industry, much research has been done on the mechanisms of fouling and which phenomena dictate its different steps. However, due to the complexity of the involved components and the process, much is still unclear. Milk is comprised of a mixture of proteins, salts, sugars, and fats. The proteins are chiefly responsible for fouling [3] and at high temperatures salts precipitate out of solution and contribute to the fouling layer. Therefore, fouling is often divided into three distinct steps: (1) the initial monolayer adsorption, (2) the growth of the fouling through the addition of aggregates to the surface and (3) the evolution of the fouling layer when the layer is heated for a prolonged period [12].

This thesis focuses on the first step in fouling: the initial adsorption of a monolayer of protein onto the steel surface. Competing theories exist on the driving force of the adsorption. Previous work done at *NIZO food research* has suggested that there is relation between the charge of the surface, the charge of the adsorbent and the amount of adsorption [13]. An opposite sign of charges of the surface and adsorbent would cause a maximum in adsorption though electrostatic attraction. Heat diffusers, where the majority of fouling takes place, are made from stainless steel whose surface consists of a layer of Cr_2O_3 [14]. Our novel approach is to use colloidal Cr_2O_3 to study the first step of fouling. Colloids have a large surface-to-mass ratio, making them extremely well suited for studying adsorption. The general experimental approach consists of adding well-known milk proteins to colloidal dispersions of Cr_2O_3. These dispersions are then analyzed with a variety of colloidal characterization techniques, such as analytical centrifugation, laser-Doppler electrophoresis, dynamic light scattering, optical microscopy, and UV-Vis spectroscopy. New information on the mechanism of monolayer adsorption of protein onto stainless steel is found and this rationalized through existing theories on adsorption. Finally, the phenomena that dictate the first step in fouling in the dairy industry are discussed, yielding insights that can be used to find solutions for the unwanted adsorption of food proteins on stainless steel.

2.Theory

The precise mechanism of the first step in protein fouling is still not completely understood. To gain more understanding of fouling, a closer look at the involved components is first taken**.** The adsorption of proteins on solid surfaces is a complicated process. Numerous factors influence the adsorption and desorption, and the involved proteins are complex molecules. Fortunately, protein adsorption is a well-developed field of study, which allows us to build on a wealth of knowledge. In this chapter we will expand on the introduction and discus in more detail the accepted theories on protein adsorption in the first part. In the second part discusses the properties of our experimental system and in the third part we present the theory behind some of the experimental techniques.

2.1.a Protein adsorption

Fouling can result in different types of deposit. Type A deposits are voluminous and are rich in whey proteins, contain 30-50% minerals and formed during treatment under 110 °C. Type B deposits are more compact, contain more minerals and are formed above 110 °C [15]. The type of deposit that forms depends on the temperature, heating rate, surface, flowrate and the composition of the product. Milk is comprised of fats, sugars, minerals and proteins and the specific amount of each component can result in a different type of deposit [2]. The temperature is also of great importance in determining the type and amount of deposit. However, both types of deposit have in common that the initial fouling starts with the adsorption of a monolayer of proteins, this occurs at low temperatures. This monolayer itself is not a problem for the production because it is only nanometers thick and therefore does not cause any measurable effects on the flowrate or heat transfer. The time it takes for this monolayer to form is typically referred to as the lag time or the induction time and can range from minutes to hours [15]. Unlike the monolayer, the subsequent fouling layers do negatively affect the production process. Even though most research on fouling is focused on the growth and evolution of fouling layers due to heat treatment, it is for the development of strategies for the prevention of fouling important that the formation of the initial monolayer is studied.

Protein adsorption onto solid surfaces is not only a problem in the food industry, it is also a issue in the biomedical sciences, pharmaceutical sciences and any other area were proteins are present [16]. The adsorption of proteins is a very common event, but also a very complicated event. The complexity of the involved materials causes a large number of factors to be relevant. To understand why and how proteins adsorb these all have to be taken into consideration. Temperature, ionic strength, the character of the surface, and pH have all been shown to affect protein adsorption [16]. Giving rise to multiple explanations for protein adsorption, including attributing hydrophobic forces, Van der Waals forces and electrostatic interactions.

For the case of the adsorption of milk proteins onto stainless steel, which we model with Cr_2O_3, the pH dependence of fouling gives an indication on which phenomena are relevant [12]. The pH determines the electrostatic state of the proteins and of the surface. Proteins contain a large number of residues that can be charged. When the pH sis equal to the isoelectric point, IEP, of the protein, there are as many positive charges as negative charges. The total net charge of the molecule is then zero. If the pH is above the IEP point the proteins have an overall negative charge whereas they have an overall positive charge below the IEP. Metal oxide surfaces contain hydroxyl groups, these group can accept or donate a proton [17]. In water a pH dependent amount of positive or negative charges are present surface of Cr_2O_3. Cr_2O_3 in the same manner as a protein has an IEP. Typical values for the IEP of a protein are 4-5 pH [18] and the IEP of stainless steel has been reported to be around pH 3 [19]. Work on the adsorption of bovine serum albumin, BSA, onto mica has shown that the adsorption is pH dependent. They found more adsorption below the IEP of BSA, where BSA is positively charged and mica is negatively charged [20]. However, research on the adsorption of β-lactoglobulin has found adsorption above its IEP onto negatively charged surfaces [21]. It is still not entirely clear to what extent electrostatic interactions dominate the adsorption behavior of milk proteins. Maximum

fouling is observed between the IEPs of the protein and the surface which leads to suspect that the electrostatic have an important role in the adsorption. In Figure 1 the surface charge of proteins and the surface is shown as a function of the pH. If electrostatic interactions are dominant for the adsorption, we would expect a strong effect of the pH on monolayer formation. The adsorption behavior can be studied in a number of ways. Adsorption isotherms are often used to quantify adsorption, the meaning and construction of these will be explained in the next chapter.

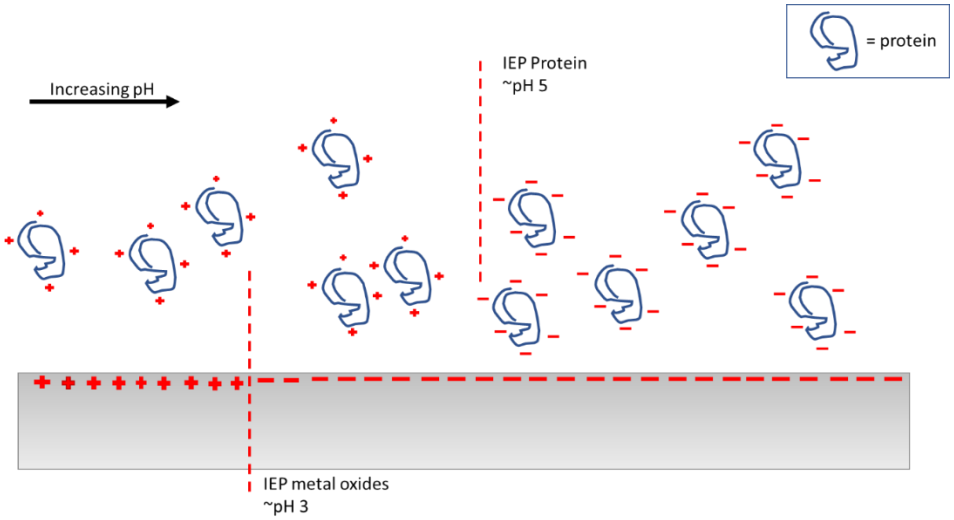

Figure 1 Schematic drawing of the surface charges on proteins and metal oxides as a function of the pH.

2.1.b Adsorption models

To characterize adsorption phenomena, adsorption isotherms have been the standard method in the literature [16], [22], [23]. In an adsorption isotherm the adsorbed amount of molecules is plotted as a function of the concentration of the free molecules in solution. Information on the in the interactions between the adsorbent and adsorbate can be gained from the adsorption isotherm . Multiple adsorption models are available for plotting experimental data [22]. Depending on the chosen model, different conclusion on the adsorption behavior can be found. Therefore, care must be taken when selecting an adsorption model.

In the field of protein adsorption the Langmuir adsorption model has long been the dominant model for describing protein adsorption. However, the Langmuir adsorption model has four criteria that have to be met before it is valid [24]. Only if these conditions are met, it is possible to reach accurate conclusions on the adsorption phenomena from the adsorption isotherm. For the Langmuir model, the conditions are:

1) All adsorption sites are identical.
2) Each adsorption site can bind one solute molecule.
3) Adsorption is reversible.
4) There are no interactions between solute molecules once they are adsorbed.

The Langmuir adsorption isotherm describes at which concentration of free molecules a monolayer of particles adsorb onto a surface depending on an equilibrium constant. The coverage is denoted with θ and has a maximum of 1 at which a full monolayer has been formed and can be further defined as:

$$\theta = \frac{q}{Q}$$

(1)

Here q is the adsorbed amount and Q the adsorbed amount where all sites are occupied. The concentration, C, is the free solute molecule concentration and k_{eq} is the combined equilibrium constant for adsorption and desorption. The Langmuir adsorption isotherm is then defined as follows:

$$\theta = \frac{Ck_{eq}}{1 + Ck_{eq}}$$

(2)

In Figure 2 the Langmuir isotherm is plotted. The θ goes to maximum of 1, a full monolayer, at high free solute concentration. The θ is not always experimentally accessible. Eq. (2) can be rewritten as:

$$q = Q\,\frac{Ck_{eq}}{1 + Ck_{eq}}$$

(3)

Of interest is the equilibrium constant because it gives us information about the free energy of the system through [24]:

$$k_{eq} = e^{-\frac{\Delta G^0}{RT}}$$

(4)

Here ΔG^0 is the Gibbs free energy of adsorption, R the gas constant and T the absolute temperature. The Gibbs free energy of adsorption describes the strength of the interaction of the adsorbate with the surface. However, we have already addressed the conditions that have to be met to apply Eq. (2). Our hypotheses is that electrostatic interactions determine whether adsorption is favorable or not. On the molecular scale, electrostatic interactions are long distance interactions [25]. The force between two charged particles scaling with r^{-2} [26] compared to the Van der Waals forces that scale with r^{-6} [27]. From the presence of charged residues in the involved proteins[28] and the presence of charged groups on a metal oxide surface [17], we know that electrostatic interactions are present. Therefore, one of the conditions for the use of Eq. (2) is not met. The adsorbed molecules will have lateral interactions so that the interaction between surface and adsorbent will change with surface coverage and the adsorption isotherm will no longer be accurately described by Eq. (2).

However the Langmuir model, Eq (2), can be adjusted to more accurately describe the adsorption behavior. Through interactions between already adsorbed molecules, the equilibrium constant is not constant. We assume that electrostatic attraction between the surface and adsorbents causes the adsorption. The already adsorbed molecules have the same charge as the molecules in solution. Therefore, if the surface is sufficiently covered, the electrostatic interactions between already adsorbed molecules and molecules in solution would alter the equilibrium constant. By assuming two regions: (1) a region where the adsorption is irreversible, (2) a region where the equilibrium constant is more favorable for desorption and thus adsorption is reversible, Eq (2) can be altered. We then define the altered Langmuir model as:

$$q = Q_{irr} + Q\,\frac{Ck_{eq}}{1 + CK_{eq}}$$

(5)

Here Q_{irr} is the irreversible adsorbed amount. Eq. (5) is plotted against the free solute concentration in Figure 3.

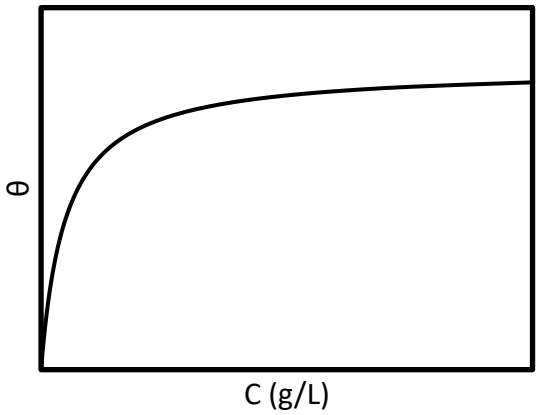

Figure 2 The Langmuir isotherm. θ goes to value of 1 for high solute concentrations.

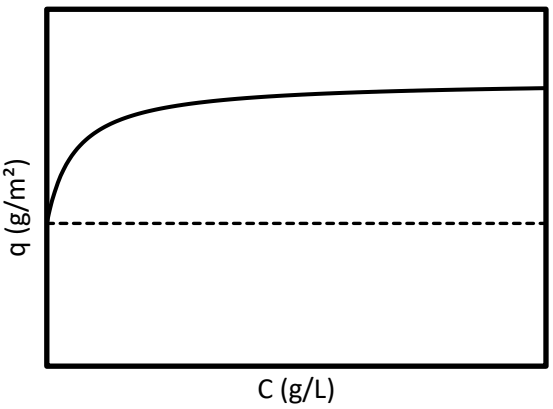

Figure 3 The Langmuir isotherm with an irreversible amount of adsorbent. The dotted line is Q_{irr}

The Langmuir model is the most common adsorption model but other models are available. One such model is the Freundlich isotherm. The Freundlich isotherm is an empirical model and is described with the following equation [22]:

$$q = KC^{1/n} \quad (6)$$

Here q is the adsorbed amount, K is the Freundlich equilibrium constant, C is the free solute molecule concentration and n is a correction factor. Eq .(6) is plotted against the free solute molecule concentration in Figure 4. However, the Freundlich isotherm is unlike the Langmuir model not based on a physical model. This means that the equilibrium constant and the correction factor are only relevant for the plotting of the experimental data and do contain more information on the adsorption behavior. Even though Eq. (6) is not based on physical model, information can still be gained from it. Because, when experimental data can be accurately fitted onto Eq (6) it is an indication that the adsorption sites are heterogeneous [29].

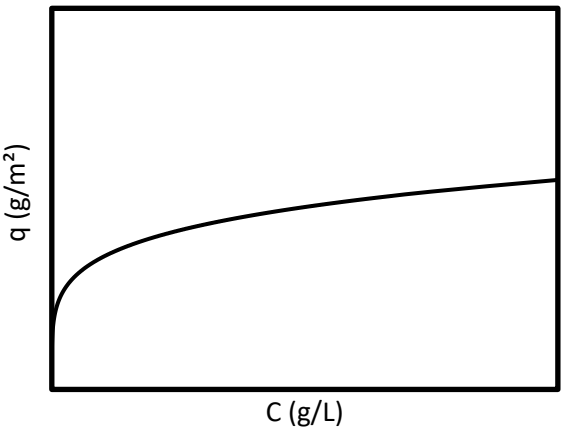

Figure 4 The Freundlich adsorption isotherm.

2.2 Properties of our experimental system

For understanding protein adsorption onto a surface three factors are the most influential: (1) External factors as in the environment, (2) the surface properties, (3) and the internal structure and properties of the adsorbate, the protein. In this chapter we discuss the protein and surface properties. The implicit effect of the environment are also discussed.

2.2.a Protein folding and residues

Proteins are an extremely complex class of materials, but they are also very common. Comprised of 20 amino acids and generally hundreds of residues long. They provide an interesting challenge when trying to understand processes where they are involved. For this thesis, the proteins present in In this research we focus on two groups of protein that are found in cow's milk, whey proteins and caseinates. Extensive work has been done on the characterization of the proteins in cow's milk.

Caseins comprise by weight ~80% of the proteins in cow's milk. In milk caseins, together with calcium phosphates form micelles. Giving due to characteristic white color of milk. For this research caseins are used in a different form. Caseins are resalted with sodium ions to form sodium caseinates. Caseins in milk are divided in four proteins fractions: α_{S1}-, a_{S2}-, β- and κ- caseins [18]**.** Caseins are phosphoproteins, which means that they contain a relatively large number of prolines [30]. All caseins posses charged groups and contain hydrophilic regions and hydrophobic regions. The formation of α-helices and β-sheets is prevented by the presence of proline in a cyclic amine side chain of caseins [31]. This results in caseins not having a set secondary or tertiary structure. Making them a class of unfolded proteins. In Table 1 properties of individual casein proteins are reported.

Approximately 20% of proteins present in cow's are whey proteins. This group of proteins is characterized as globular, folded, proteins. They have complex secondary and tertiary structures, this is opposed to caseins. Whey proteins consist of a number of proteins, including: α-lactalbumin, β-lactoglobulin, immunoglobulins, bovine serum albumin, and numerous enzymes are present in smaller amounts [32]. The focus is on α-lactalbumin and β-lactoglobulin as they are the main participating proteins in fouling [12] and the largest protein fractions in whey protein. Both are tightly folded proteins and the secondary structure is relatively insensitive to pH changes. α-lactalbumin has tightly folded structure [33] and is present as a monomer. β-lactoglobulin contains a free thiol group in it structure which is suspected to chemically bind to metal surfaces at high temperatures [3]. β-lactoglobulin is mostly found as dimer in nature but can also form monomer or oligomers depending on the pH [34]. At low pH the monomer form is dominant while near the IEP oligomers are found and at higher pH values dimers. In Table 1 more properties of α-lactalbumin and β-lactoglobulin are reported.

Table 1 selected properties of caseins and whey proteins

Protein	Mass (kDa)	IEP (pH)	Fraction	reference
Caseins	-	4.6	~80%	[18], [35]
α_{s1}-casein	23.6 kDa	4.2-4.6	31%	[18], [35]
α_{s2}-casein	25.2 kDa	-	8%	[18]
β-casein	24,0 kDa	4.6-5.1	29%	[18], [35]
κ-casein	19.0 kDa	4.1	32%	[18]
Whey proteins	-	4.9	~20%	[18]
β-lactoglobulin	18.4 kDa	5.35-5.49	55-65 %	[36]
α-lactalbumin	14.2 kDa	4.2-4.5	15-25%	[36]

2.2.b Solid surface properties

The interest of this research is the protein adsorption at the liquid/solid interface. The solid interface is the surface of Cr_2O_3. Cr_2O_3 is a crystalline material with a rhombohedral crystal lattice [37]. The exact properties of the surface depend on the terminal facet of the crystal [38]. The general characteristics are similar, regardless of the terminal facet and with a polycrystalline sample of Cr_2O_3 the effect will be averaged. There is large difference between the dielectric constant of Cr_2O_3 [39] and of water [40] form which we expect relatively strong Van der Waals interactions predicted by Lifshitz theory [41]. Furthermore, the surface oxygen molecules form hydroxyl groups when Cr_2O_3 is exposed to water [42]. The hydroxyl groups serve as cation and anion exchange sites which are the origin of the surface charge [17]. The surface charge dictates the electrostatic interactions with the surroundings of Cr_2O_3 particles. How the surface charge is characterized is discussed in the next paragraph.

2.2.c Zeta potentials of solids and proteins

In this paragraph, a concise overview of theory behind the zeta potential is presented based on the book *Basic Principles of Colloid Science* by D.H. Everett [43]. The significance of electrostatic interactions in colloid science cannot be overstated, as they are the origin of many of the defining characteristics of colloids, including the surface charge. The zeta potential is a measure of the surface charge. Colloidal stability is often discussed in relation to surface charge, where a higher surface charge indicates greater stability [44]. Moreover, surface charges have a direct impact on the adsorption behavior of charged particles. Generally, particles with a surface charge are not expected to adsorb onto a charged surface with the same sign of charge unless there is a stronger force driving the adsorption. Therefore, to correctly interpret the interactions between proteins and Cr_2O_3 their surface charges have to be characterized.

In colloidal chemistry, surface charge is usually characterized by determining the zeta potential. In contrast to the surface charge, the zeta potential is easily accessible experimentally through electrophoretic mobility measurements. The electrophoretic mobility is the velocity of the charged particles caused by the application of an electric field and is defined as [43], [45]:

$$\mu_e = \frac{2}{3}\frac{\varepsilon_0 \varepsilon_r}{\eta}\zeta f(\kappa a) \tag{7}$$

here the charge of the particle is accounted for by the zeta potential, ζ. $\varepsilon_0\varepsilon_r$ is the electric permittivity of the medium, η is the viscosity and $f(\kappa a)$ is the Henry function. We will first discuss in more depth the definition of the zeta potential before we touch on the meaning of the Henry function. Upon dispersing particles in an aqueous medium, almost instantaneously an electric double layer, EDL, is formed. This is caused by electrically charged groups disassociating from the surface and the equilibrium between the charged particle and counter ions that is then formed. DLVO theory describes the formation of the EDL [46]. For our purposes it is enough to know that the EDL is described as being comprised of two regions: a stationary layer and diffuse layer. The zeta potential is the potential of the electric double layer at the slipping plane. The slipping plane is defined as the plane of shear between the diffuse layer and the stationary layer. The location of the slipping plane, and thus the zeta potential, depends on the cut-off for the stationary layer. The exact location of this plane depends the on the hydrodynamic radius, a, and the reciprocal Debye screening length, κ . The Debye screening length is defined as [47]:

$$\kappa^{-1} = \sqrt{\frac{\varepsilon_0 \varepsilon_r k_B T}{2e^2 I}}$$

(8)

where $k_B$is the Boltzmann constant, T is the temperature, e is the elementary charge, and I is the ionic strength. The ionic strength is the summation of all ions present times the square of their valency. The ratio between the electrophoretic mobility and the zeta potential depends on the Henry function. The Henry function connects two approximations, The Hückel approximation and Helmholtz-Smoluchowski approximation. The Hückel approximation is applied if $\kappa a < 0.1$, which is the case for small particles at low ionic strength, in this limit $f(\kappa a) \rightarrow 1$. If $\kappa a > 100$, the Helmholtz-Smoluchowski approximation is used and $f(\kappa a) \rightarrow {}^{3}/_{2}$. This is the case for large, ~1 μm, particles at high ionic strength. For our purposes, it is important to remember that the zeta potential is a measure of the surface charge. But care must be taken when interpreting electrophoretic mobility measurements because the ionic strength and the particle radius influence the size of the zeta potential.

2.3 Experimental characterization techniques

2.3.a Nitrogen physisorption

To compare adsorption data with the literature in terms of grams per square meter, it is necessary to accurately determine the surface area. For non-uniformly shaped particles the surface area is not easily accurately determined with optics. A standard way to determine the surface area is nitrogen physisorption. Nitrogen is used as a probe molecule and by calculating the total number of molecules that is used to cover a sample with a monolayer, the total surface area can be determined. This is done by placing a sample in a vacuum chamber at the boiling point of nitrogen. Precisely measured amounts of nitrogen are added to the chamber. This increases the pressure in the chamber and according to the ideal gas law we would expect a linear increase in pressure but physisorption of nitrogen onto the sample causes the pressure to increase non-linearly. Nitrogen is added until p_0 is reached which is the boiling pressure for nitrogen at 77 K. The pressure is then lowered till a vacuum is reached again. This creates an adsorption isotherm and a desorption isotherm. If the sample is porous hysteresis will be found between the adsorption and desorption isotherm. The shape and size of the hysteresis contains information on the type and size of the pores in the sample.

The surface is determined from the adsorption isotherm with the BET model [48] [49]. The BET model builds on the Langmuir adsorption model but BET model accounts for the formation of multilayers of nitrogen onto the surface. From this model an equation for an isotherm is formulated that can be used to determine the surface area.

$$v = \frac{v_m c p}{(p_0 - p)(1 + (c - 1)(p/p_0))}$$

(9)

Here v is the volume of the added nitrogen gas and p the measured pressure. c is the BET constant and is the ratio between adsorption strength of a monolayer and the adsorption strength of the subsequent layers. v_m is the volume of the monolayer of nitrogen molecules. For the determination of the surface area the isotherm is fitted onto the region where $p \ll p_0$ and to fit the experimental data Eq. (9) is written in the linear form:

$$\frac{p}{v(p_0 - p)} = \frac{1}{v_m c} + \frac{c - 1}{v_m c}\frac{p}{p_0}$$

(10)

This linear equation is useful since a plot of this equation will have a y-intercept of $1/v_m c$ and a slope of $(c-1)/v_m c$. From here the v_m and c can be determined. The number of nitrogen molecules in the adsorbed monolayer is calculated. Knowing the surface per nitrogen molecule and the mass of the sample, the surface area per gram of sample is determined. This is the BET surface area and is commonly used to report the surface area of a material.

2.3.b Analytical centrifugation

One way to determine the particle size distribution, PSD, is through analytical centrifugation. Analytical centrifugation has long been a trusted tool in colloidal chemistry and has been successfully used to determine PSDs from all manner of dispersed colloidal particles [50][51]. In our research the PSD is of interest because it is an indicator of the degree of aggregation [52]. The definition of a stable colloidal dispersion in which the particles are not aggregated. Preliminary work has shown that the addition of proteins the colloidal dispersions stabilizes them [13]. This stabilizing effect of proteins can be explained by the steric repulsions caused by adsorbed proteins [53]. By calculating the particle size distribution, the stabilizing effect of proteins on colloidal dispersions can be quantified. The extent of the stabilization can then be linked to protein adsorption.

The sedimentation velocity is experimentally determined. To find the corresponding particle size the forces to which the particle is subject to are examined. We assume that only the centrifugal force, a friction force, and the buoyant force work on the particles, neglecting interactions between particles, diffusion and the gravitational force. Interactions between particles can be neglected as long as the sedimentation velocity is measured in the region where the particles are not too concentrated. For the diffusion and the gravitational force the assumption that they can be neglected is valid as long as the centrifugal force, and resulting velocity, are much greater than the gravitational force and any effects caused by diffusion. The force balance is then defined as:

$$F_{friction} = F_{centrifugal} \tag{11}$$

The balance between these forces is nearly instantaneously reached. The centrifugal force is defined as:

$$F_{centrifugal} = \Delta m \omega^2 r \tag{12}$$

with Δm the buoyant mass, ω the radial velocity and r the radius of rotation. The radius of rotation is assumed to be constant and equal to the radius of the centrifuge. The buoyant force is integrated into this definition of the centrifugal force by using the buoyant mass, Δm. The buoyant mass is the difference in density between the solvent and the particle times the volume of the particle:

$$\Delta m = V\left(\rho_{particle} - \rho_{solvent}\right) = \frac{4}{3}\pi a^3 \Delta\rho \tag{13}$$

where a is the radius of the particle which we assume is equal to hydrodynamic radius. This assumption is valid if the particles are roughly spherical. $\Delta\rho$ is the effective density of the particle. We then obtain from combining Eq. (11) and Eq. (12):

$$F_{centrifugal} = \frac{4}{3}\pi a^3 \Delta\rho \omega^2 r$$

(14)

This is one half of our force balance. The other side of the force balance is the determined by the friction force which we define as the Stokes' friction factor times the velocity [54]:

$$F_{friction} = f_{Stokes} v = 6\pi a \eta v$$

(15)

with a the hydrodynamic radius, η the viscosity and v the sedimentation velocity. The Stokes' friction factor for spherical particles is used. The assumption of by approximation spherical particles is validated with transmission electron microscopy. By filling in Eq. (13) and Eq. (14) in Eq. (10) we find:

$$6\pi a \eta v = \frac{4}{3}\pi a^3 \Delta\rho \omega^2 r$$

(16)

We can rewrite Eq. (15) to a function for the radius because the radius of the particle is assumed to be equal to the hydrodynamic radius:

$$a = \sqrt{\frac{9}{2}\frac{\eta v}{\Delta\rho\omega^2 r}}$$

(17)

The sedimentation velocity, v, is experimentally determined and the effective density, radial velocity and the radius of the centrifuge are known. The sedimentation velocity is defined as:

$$v = \frac{\Delta x}{\Delta t}$$

(18)

where the change in position for a fraction with one absorbance value is measured. For a monodisperse sample, one sedimentation velocity will be found. For a polydisperse sample a distribution of sedimentation velocities will be measured. The sedimentation velocities are calculated per absorbance fraction. To find the size distribution, in other words the probability function of the size, the first derivative of the following cumulative function is taken: total absorbance against the sedimentation velocity. The reason for this is that the cumulative absorbance scales with the amount of particles (the total volume of colloidal material) and the sedimentation velocity, a measure of the size of the particles. We take the derivative of this function to find the distribution of the sedimentation velocities.

$$\mathrm{P}(v) = \frac{\mathrm{d}A}{\mathrm{d}v}$$

(19)

This is done numerically in Python, where the probability values of discrete sedimentation velocities are calculated. A plot is then generated of the probability value against the corresponding sedimentation velocity. With Eq. (16) the sedimentation velocity is related to the hydrodynamic radius. Resulting in

probability values for the radii of the particles. This is particle size distribution. To find a function that describes this distribution, the data points are fitted on a log-normal distribution.

By assuming a log-normal distribution of the particles, the distribution can be expressed with an average size and a standard deviation. Log-normal distributions are often used to describe the distribution of colloidal particles[52], [55]. The probability density function for the log-normal distribution is defined as [56]:

$$f(a) = \frac{1}{a\sigma\sqrt{2\pi}} e^{-\frac{1}{2}\left(\frac{\ln(a)-\mu}{\sigma}\right)^2}$$

(20)

where a is log-normal distributed value. σ the standard deviation of log-transformed data and μ the mean of log-transformed data. These are not the same as the mean and standard deviation of the data and must be transformed before being interpreted. Otherwise, they are only scaling parameters for the log-normal distribution. The mean of the normal population is then calculated with[57]:

$$\text{Mean}(a) = \exp\left(\mu + \frac{1}{2}\sigma^2\right)$$

(21)

And the variance, the square of the standard deviation, is:

$$\text{Variance}(a) = (\exp(\sigma^2) - 1)\exp(2\mu + \sigma^2)$$

(22)

The μ and σ are found by fitting experimental data on log-normal distribution. The particle size distribution can then be represented by two variables, the mean and standard deviation. By summarizing the particle size distribution with two parameters the effect of a change in pH on the extent of the stabilization can be examined.

2.3.c Dynamic light scattering

Dynamic light scattering, DLS, is another powerful method for the determination of particle size distributions. Frequently used in colloid science [58], [59] and biomedical sciences [59] for the determination of particle sizes in the colloidal domain. Strengths of this technique are that the particle size is measured *in-situ* compared to other characterization techniques such as electron microscopy. Furthermore, by definition a very large number of particles is used to determine the PSD which provides a robust statistical average. Drawbacks are that samples must be dilute to prevent multiple scattering and because DLS uses the intensity of scattering, larger particles are heavily favored. This second drawback makes it crucial that samples are dust free, as large dust particles would dominate the PSD. We give a very brief overview of the theory behind DLS here, to provide theoretical basis on which we compare DLS PSDs to PSDs calculated with analytical centrifugation.

DLS is based on two characteristics of the colloidal particles, their scattering and Brownian motion. A monochromatic and coherent beam of light is shone through a sample containing colloidal particles. The intensity at a specific angle (173° for large particles) is measured as a function of time. The changes in intensity are related to motion of the particles with an autocorrelation function. The motion of colloidal particles is the Brownian motion. Brownian motion depends on the translational diffusion coefficient of the particles. Which is defined with the Stokes-Einstein relation as[60]:

$$D_t = \frac{kT}{f_{Stokes}}$$

(23)

where k is the Boltzmann constant, T is the temperature and f_{Stokes} is the same friction factor as in Eq (14). This allows us to directly compare radii from DLS with the radii from analytical centrifugation.

2.3.d UV-Vis spectroscopy

UV-Vis spectroscopy is a sensitive, low cost and non-invasive method for the characterization and quantification of UV-Vis active components in solution. Proteins are extremely suited for analysis with UV-Vis spectroscopy because they strongly absorb light at 280 nm. This is due to the presence of the residues tryptophan, tyrosine, and in a lesser capacity phenylalanine [61]. The difference between the intensity of a reference beam and the intensity of beam of light that passed through the sample is analyzed. Where intensity of the sample beam is equal to the reference beam if there are no absorbing species in the sample. This is called the transmittance and is defined as follows:

$$T = \frac{I}{I_0}$$

(24)

The absorbance, or more strictly speaking the optical density, is then defined as:

$$A = -log_{10}\left(\frac{I}{I_0}\right)$$

(25)

The absorbance only accounts for the extinction of light through absorption by components in the sample. The optical density is given by the same formula but accounts for absorption and scattering. The absorption is directly proportional to the concentration of absorbing components times a coefficient and the optical path length. The following equation is commonly known as Lambert-Beer's law [62]:

$$A = \varepsilon c l$$

(26)

ε is the extinction coefficient, c, the concentration and l the path length. The extinction coefficient is readily experimentally determined with a calibration series and the path length is known. The concentration is the value that is of interest. Lambert-Beer's law can be applied as long as the sample is dilute, scattering is limited, and absorbing species do not interact. In samples without any contaminants the concentration is then accurately determined by comparing the absorption at one wavelength with a calibration series. If the sample consists of more than one UV-Vis active component with overlapping absorption peaks, more steps are necessary to determine the concentration of the components. This can be solved because Lambert-Beer's law holds at any given wavelength. This can be written down as:

$$A_i = k_i c$$

(27)

The subscript i denotes the wavelength and the factor k_i is the product of the wavelength specific extinction coefficient, ε_i , and the pathlength, l. The different extinction coefficient per wavelength gives rise to a

characteristic spectrum. If there is more than one UV-Vis active component present, the absorption is the sum of the absorption of n components:

$$A_i = \sum_n k_{in} c_n \tag{28}$$

This can also be notated in the matrix form:

$$\begin{bmatrix} A_1 \\ A_2 \\ \cdots \\ A_i \end{bmatrix} = \begin{bmatrix} k_{11}c_1 & + & k_{11}c_2 & + & \cdots & + & k_{1n}c_n \\ k_{21}c_1 & + & k_{21}c_2 & + & \cdots & + & k_{21}c_n \\ \cdots & + & \cdots & + & \cdots & + & \cdots \\ k_{i1}c_1 & + & k_{21}c_2 & + & \cdots & + & k_{i1}c_n \end{bmatrix} \tag{29}$$

which can be written as,

$$A = Kc \tag{30}$$

K is the matrix containing the pure spectra of the components, A the vector with measured absorbance at each wavelength and c the vector with the unknown concentrations of n pure components. Notated in matrix form:

$$A = \begin{bmatrix} A_1 \\ A_2 \\ \cdots \\ A_i \end{bmatrix}, \qquad K = \begin{bmatrix} k_{11} & k_{12} & \cdots & k_{1n} \\ k_{21} & k_{22} & \cdots & k_{2n} \\ \vdots & \vdots & \ddots & \vdots \\ k_{i1} & k_{i2} & \cdots & k_{in} \end{bmatrix} and \qquad c = \begin{bmatrix} c_1 \\ c_2 \\ \cdots \\ c_n \end{bmatrix} \tag{31}$$

Knowing K and A we can calculate the concentrations, c_n, for all components. The K is determined by measuring pure reference spectra with a known concentration. There is an exact solution for Eq. (29) if there is no noise in the signal and there are no unaccounted-for components. In practice this not possible; however, with the classical least squares method, CLS, the solution can be approximated. CLS minimizes the square of the error between the measured absorbance and the calculated absorbance. This is done by varying the weight of the components in c. Limitations on the allowed solutions can be set, such as disallowance of negative values for components. This is variant of CLS is called non-negative least squares, NNLS, method. For our purposes, this allows the determination of protein concentrations even when the spectra of other UV-Vis active components overlap with the spectrum of interest. Python modules are available to implement NNLS. Above method is derived largely from a blogpost by Nicolas Coca on Quantitative Spectral Analysis, here a full derivation of the CLS is also given [63] and on Quantitative Chemical analysis by D. Harris [64].

3. Materials and methods

3.1 Materials

Chromium(III) oxide, (Cr_2O_3, ultra dry) was purchased from Sigma-Aldrich and used as received. Bipro, (whey proteins) and NaCas (sodium caseinates) were provided by NIZO and used as received. Approximate compositions of the used whey protein and NaCas are listed in Table 2 below [13]. Sodium phosphate dibasic (Na_2HPO_4, ≥99.0%), sodium phosphate monobasic dihydrate ($NaH_2PO_4 \cdot 2H_2O$, ≥99.0% (T)), hydrochloric acid (HCl, fuming 37% sol), and sodium hydroxide (NaOH, ≥98.0%) were purchased from Sigma-Aldrich and used as received. Potassium dichromate(VI) ($K_2Cr_2O_7$, ≥99.5%) was purchased from Fisher Scientific and used as received. In all experiments MilliQ water (18.2 MΩcm at 20 °C) was used.

Table 2 composition of NaCas and whey protein in % of proteins

Protein mixture	Protein	Abundance
NaCas	α_{s1}-casein	31%
	α_{s2}-casein	8%
	β-casein	31%
	κ-casein	10%
Whey proteins	β-lactoglobulin	80%
	α-lactalbumin	20%

3.2 Methods

3.2.a. Colloidal stability analysis

Sample preparation for colloidal stability analysis

A buffer solution of 0.1 M sodium phosphate was used for all samples. Phosphate buffer was made by adding 3.287 g of Na_2HPO_4 and 2.649 g of NaH_2PO_4 to 400 mL MilliQ, the buffer had a pH of 6.97. The Buffer was brought to required pH with HCl and NaOH and pH was determined with a negative electrode probe with a pH meter (Seven Excellence, Mettler Toledo). All samples were prepared with 2 wt% Cr_2O_3 and 0.5 wt% protein. Proteins that were used were NaCas and whey proteins. The pH was varied between 3 and 7 with steps of 0.5 pH unit. The samples were prepared in batches and with the following order of operations. 100 mg of Cr_2O_3 powder was added to a 10 mL counting vial; subsequently 3.9 g of buffer at the required pH was added and then 0.5 g of 5 wt% protein stock. The protein stock was prepared by dissolving protein in buffer at pH 7. The sample was then vortex mixed to ensure all of the Cr_2O_3 surface had been exposed to the protein. Samples were stored at 4 °C to prevent spoilage of the proteins.

Colloidal stability analysis

The colloidal stability was measured with the LUMiSizer. The LUMiSizer is a slow analytical centrifuge with the ability to measure the time resolved transmission over the length of a cuvette. Samples were redispersed before measuring with a vortex mixer. ~0.5 mL of sample was added to a plastic disposable LUMiSizer cuvette and centrifuged at 400 rpm (23 *g*) for 40 minutes. The transmission was measured at 865 nm every 10 seconds at 255 positions along the cuvette. The temperature was kept at 20 °C during all measurements. Two reference measurements were performed, one with cuvette with water for a 100% transmission measurement and 0% transmission with a cuvette filled with a cut-to-size piece of black paper. We determined the particle size distribution from the LUMiSizer transmission data with a custom Python script. In Appendix I the data processing with Python code is explained. In this way, we obtained a transmission weighted particle size distribution. This distribution is fitted on log-normal distribution in Excel. For the fit in Excel we normalize the weights of the of the found radii to one. The normal log-distribution in Excel used is:

$$\text{Probability} = S * \text{LOGNORM.DIST}(a, \mu, \sigma, \text{FALSE}) \quad (32)$$

where a is the found radius, μ is the mean of $\ln(a)$, σ is the standard deviation of $\ln(a)$ and the clause FALSE ensures that a probability function is used. S is a scaling factor that we added because the data set that we fit on is incomplete. The data sets are incomplete because the radii of the particles were calculated for a limited number of sedimentation velocities. A fit was generated by minimizing the cumulative sum of the residuals between the found distribution weights and the calculated weights by adjusting the parameters S, μ and σ with the solver plugin. Obvious outliers caused by artefacts of the data processing were removed before fitting. An R^2 value was calculated to judge the quality of the fit; typical R^2 values found were above 0.98. The mean and standard deviation were converted to mean and standard deviation of the normal population. The mean of the normal population was found with Eq. (20) and the variance, which is the standard deviation squared, was calculated with Eq. (21). The average size and standard deviation found with log-normal distribution were plotted against the pH.

3.2.b Adsorption isotherms

Sample preparation for adsorption isotherms

A stock solution of protein was prepared at pH 7 with a concentration of 2 wt% in milliQ water. Experiments were performed in 2 mL Eppendorf tubes. Samples were prepared in batches. The concentration of Cr_2O_3 was kept constant at 4wt%. Samples were brought to the required total volume with MilliQ water at pH 3, pH 5 or pH 7. The protein concentration was varied from 0.01 wt% to 0.1 wt% (approx. 10 mg/L to 1000 mg/L) by adding concentrated protein stock. Samples were then thoroughly mixed with a vortex mixer to ensure the complete surface had been exposed. Samples were left overnight to make sure an equilibrium had been reached. Cr_2O_3 particles were separated by centrifuging at 14800 rpm with a tabletop centrifuge (Microfuge). The supernatant was then analyzed with UV-Vis spectrometer (PerkinElmer, Lambda 365+) to quantify the remaining protein concentration. Undiluted samples were placed in a 10 mm quartz cuvette (Hellma analytics) and analyzed between 200 and 700 nm. Reference spectra of 10 times diluted stock was measured for each batch. The quartz cuvettes were flushed thrice with MilliQ water and thrice with ethanol and were then dried with pressurized nitrogen between measurements and.

Sample preparation reversibility experiments

The reversibility of adsorption was tested by washing the samples with MilliQ water and analyzing the amount of protein in the supernatant. Experiments were performed in 2 mL Eppendorf tubes. Samples containing 4 wt% Cr_2O_3 and 0.1 wt% protein at pH 7 were examined. Samples were washed three times. The concentration in the supernatant of the unwashed protein was analyzed to determine the initial adsorbed amount. For the first wash, the sample was redispersed in fresh water at pH 7 and left to reach equilibrium for one hour. After one hour the sample was centrifuged at 14800 rpm and the supernatant was analyzed. This was repeated for a total of three times. For the last wash the sample was left to equilibrate overnight before centrifuging and analyzing supernatant.

Data processing of UV-Vis spectra

The Cr_2O_3 colloidal powder was used as received from Sigma-Aldrich. UV-Vis spectroscopy showed that the Cr(III) was contaminated with Cr(VI). Cr(VI) was present in two hydration forms , $HCrO_4^-$ and CrO_4^{2-} , at low concentrations and moderate pH [65]. Both these Cr(VI) species absorb strongly in the near UV and visible spectrum [66]. These contaminants proved to be difficult to wash away and therefore we filtered out the absorption by Cr(VI) using a Python script. This code was written inspired by a blog post by Nicolas Coca on quantitative spectral analysis [63]. The method is based on the classical least squares method and modified to disallow negative concentrations of components as a solution and account for a scattering

background component. This method requires reference spectra of all components. Reference samples were made by making a stock solution of $K_2Cr_2O_7$ with a concentration of 30 mM. Samples for UV-Vis spectroscopy were made by diluting stock solutions 200 times to a concentration of 0.15 mM. Samples were prepared at pH 2 and pH 12. These were the reference spectra for respectively $HCrO_4^-$ and CrO_4^{2-}. The Python code is explained in Appendix II. After processing, the concentration of protein in the supernatant was determined. The adsorbed amount of protein was then calculated by comparing the initial concentration with the measured steady state concentration with the mass balance:

$$C_{ads} = C_i - C_{ss} \quad (33)$$

where C_{ads} is the adsorbed concentration, C_i the initial concentration and C_{ss} the measured concentration al in mg/L. The steady state concentration is equal to free solute molecule concentration form Eq. (2). The adsorbed amount per surface area, q, was then calculated with:

$$q = \frac{C_{ads}V}{SSA * m} \quad (34)$$

where the SSA is the specific surface area in m^2/g of Cr_2O_3. This the BET surface determined with nitrogen physisorption. V is the total sample volume in L and m is the mass of the Cr_2O_3 in the sample in g. The adsorption isotherms are then constructed by plotting q, the adsorbed amount per surface, against the C_{ss}, the steady state protein concentration.

3.2.c Optical microscopy

Preliminary work showed that colloidal Cr_2O_3 dispersions were stabilized by the addition of a protein in solution. To further examine this effect, samples were placed under an optical microscope (Nikon Ts2). A representative image was taken for a qualitative comparison between samples. The samples were 2 wt% Cr_2O_3 with 1 wt% NaCas in 0.1 M phosphate buffer, 2 wt% Cr_2O_3 with 1 wt% whey protein in 0.1 M phosphate buffer and 2 wt% in 0.1 M phosphate buffer at pH 7.

3.2.d Dynamic light scattering

Dynamic light scattering (DLS) was used to determine the particle size and distribution of Cr_2O_3 particles as a function of the pH. Samples were measured with the multi angle particle analyzer (Zetasizer Ultra Malvern). To prevent multiple scattering effects, the samples were diluted to $1*10^{-4}$ vf (volume fraction) with water. This was done by dispersing 1 mg of Cr_2O_3 in 10 mL of water and sonicating. Measurements were performed simultaneously with zeta potential measurements. A DTS1070 sample cell was used, and the sample was continuously stirred and pumped around between measurements. Sample was titrated from the starting pH to pH 2 using an auto titrator with a step size of 1 pH unit. Titrants used were 0.1 M HCl, 0.01 M HCl and 0.1 M NaOH. The temperature was set at 25 °C and per pH value three measurements were taken for error analysis.

3.2.e Transmission electron microscopy

Transmission electron microscopy (TEM) was used to examine the particle size and shape of Cr_2O_3. The effect of adsorbed proteins on Cr_2O_3 particles was also examined with TEM (Tecnai 20 FEI). Strongly diluted samples ($1*10^{-4}$-$1*10^{-5}$ vf) of bare Cr_2O_3 and of Cr_2O_3 with protein were deposited on copper grids and dried under an IR lamp for 1 hour. Images were analyzed with ImageJ software.

3.2.f. Nitrogen physisorption isotherms

Nitrogen physisorption was used to give a measure of the surface area per gram of Cr_2O_3 and the porosity. A sample of Cr_2O_3 was heated to 150 °C under vacuum overnight to drive off any remaining moisture. The mass of the sample after drying was 2.4178 g. In a vacuum chamber at 77 K nitrogen was added till p_0 was reached. The adsorption and desorption isotherms were measured by measuring the pressure in the vacuum chamber. The surface area was determined with BET method, where Eq. (9) is fitted on the adsorption isotherm where $p \ll p_0$. The selection area for the fit of the BET isotherm was 0.04 p/p_0 till 0.16 p/p_0. A cross-sectional area for nitrogen of 0.1620 nm^2 was assumed and the equilibrium time between measurements was 12 s. Measurements were performed on a Micrometrics TriStar II Plus.

3.2.g Zeta potential

The zeta potential at different pH values was measured through laser doppler electrophoresis with the Zetasizer ultra (Malvern). The zeta potential of 0.1 wt% proteins in MilliQ water was measured from pH 7 to pH 2 in. Dispersion with $1*10^{-4}$ vf Cr_2O_3 were measured in MilliQ and in 0.1 M phosphate buffer. The titrants used were HCl solutions with a concentration of 0.1 M and 0.01 M and a 0.01 M NaOH solution. Temperature was kept at 25 °C. DTS1070 sample cells were used, and the samples were continuously stirred and pumped around between measurements. 5 measurements with 120 s for equilibration between the measurements were performed for error analysis. For the double layer approximation, the automated setting of the Zetasizer was used.

4. Results and discussion

4.1 Particle size determination Cr_2O_3

For an accurate description of protein adsorption on the surface of Cr_2O_3 particles, we need to accurately know the characteristics of these particles. The main parameters of the colloidal Cr_2O_3 that we need to determine are the size and surface area of the particles. Other characteristics such as the surface charge are also of interest and have been studied. We have used three techniques to determine the size and/or surface area of the particles: transmission electron microscopy (TEM), dynamic light scattering and nitrogen physisorption.

4.1.a Transmission electron microscopy

Bare Cr_2O_3

Dilute dispersions of Cr_2O_3 were dried to examine the particles with TEM. The samples were very dilute limiting the number of particles captured with TEM. Images of four examples of bare Cr_2O_3 are shown in Figure 5 .

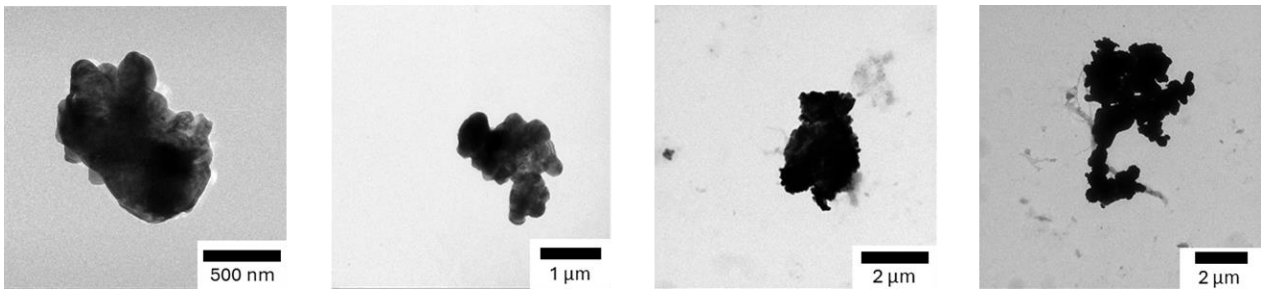

Figure 5 TEM images of bare Cr_2O_3 particles.

The particles are relatively compact but not spherical. They can better be described as potato-like, and they do not show clear facets. Larger particles are built out of smaller segments and aggregates are comprised of smaller loose particles. The segments are not uniformly sized. The dimensions of the shown particles are typically in the range between 400 and 2000 nm. . Due to the small number of particles, no PSD from the images was determined. To determine a PSD, a large number of particles is necessary to calculate a distribution representative of the total population, but the particle and segment sizes are highly polydisperse. Clusters of particles are found, which can have formed during the drying process during sample preparation or in solution earlier in the sample preparation. TEM images give a qualitative image but fail to give quantitative data in our case and furthermore, samples preparation changes the aggregation condition due to drying effects.

Cr_2O_3 with whey protein

TEM images of dispersions of Cr_2O_3 particles stabilized with whey protein were also made. The dispersions were made with an excess of protein and subsequently washed. The aim of this was to picture Cr_2O_3 particles covered with a monolayer of protein. We did not expect to be able to distinguish proteins on the surface because the proteins have a radius of 3-4 nanometers and a low mass density compared to Cr_2O_3. Particles were sonicated before taking TEM samples to obtain the maximum number of loose particles. More representative images of the PSD of Cr_2O_3 can be made in this manner. In Figure 6 strongly diluted and washed Cr_2O_3 with and adsorbed whey protein layer dispersions are shown.

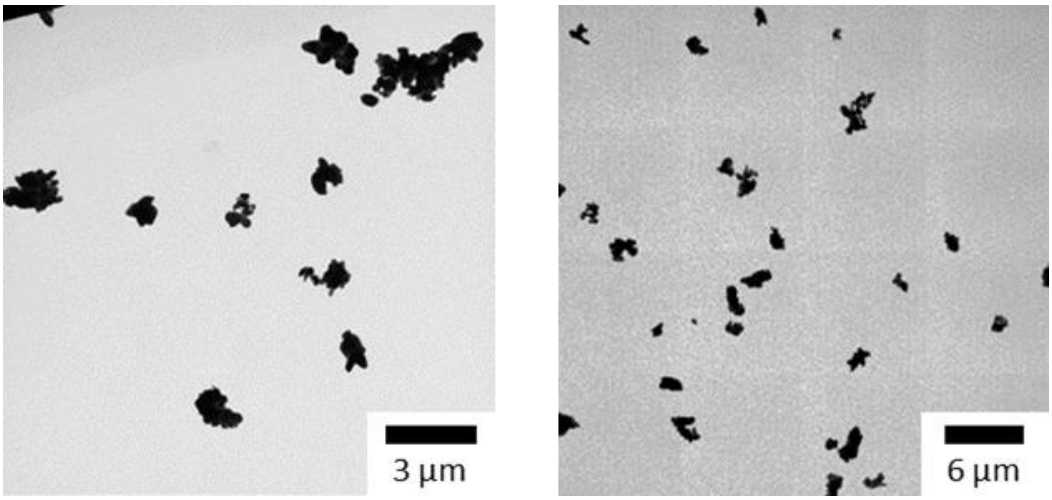

Figure 6 TEM images of Cr_2O_3 with adsorbed whey protein.

The whey protein-covered protein particles have a diameter of hundreds of nanometers. A larger number of particles could be imaged than with the bare Cr_2O_3 particles (Figure 5). The particles are comparable particles to those in Fig 5**.** The particles appear to be in stages of aggregation. From these images, the extent of stabilization by protein adsorption cannot be analyzed. TEM images do not give information on aggregation state *in-situ* since samples are diluted and dried before imaging, completely altering the environment and therefore the aggregation state of the particles.

Cr_2O_3 with NaCas

TEM images of Cr_2O_3 particles with a layer of adsorbed NaCas were made. The samples were prepared in the same manner as Cr_2O_3 with whey protein samples. The average particle size found in TEM images of Cr_2O_3 with NaCas was larger than that of Cr_2O_3 with whey protein. Aggregates found were significantly larger. In Figure 7A one such aggregate is shown and in Figure 7B a particle with a suspected protein layer is shown.

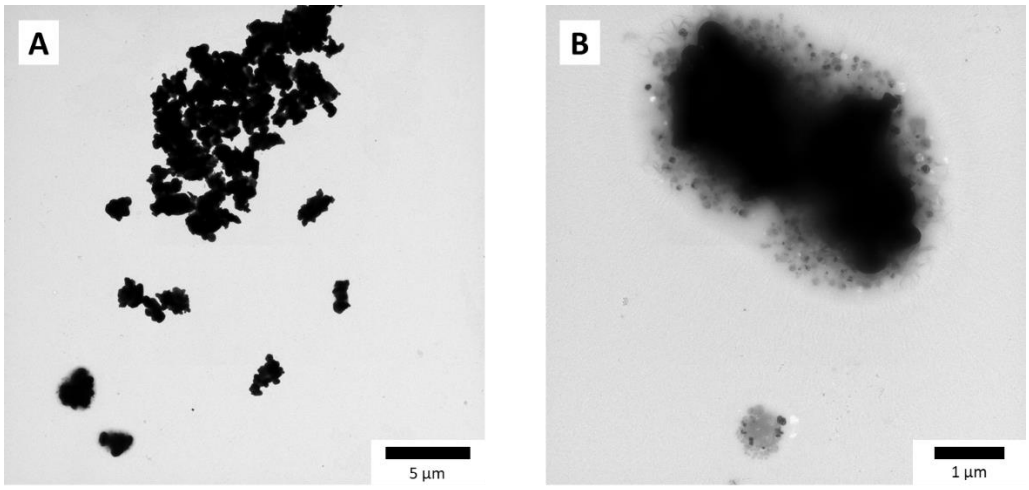

Figure 7 TEM images of Cr_2O_3 with NaCas. Figure A shows a large aggregate cluster. Figure B shows a particle with a possible protein layer..

The aggregate in Figure 7A is built out of smaller units that have a similar size as the particles shown in Figure 5. In the left bottom a particle with a fuzzy border is shown. A close up of a similar particle is shown

in Figure 7B. The diffuse layer is possibly due to a drying effect, where the caseins form a non-dense layer around the particles. It is not clear why only a fraction of the particles shows this effect. In Conclusion, the particles have an ill-defined shape, and it is difficult to determine an average size or surface area from TEM.

4.1.b Dynamic light scattering

Dilute dispersions ($1*10^{-4}$ vf) of Cr_2O_3 were analyzed through dynamic light scattering. The size of particle cluster was studied and the effect of the pH on the particle size was examined. In Figure 8 the average number weighted particle size against the pH is shown. One point is comprised of three measurements and the error bars indicate the standard deviation. There is a slight trend to a larger particle diameter at lower pH. The average particle diameter is around 700 nm, this is in the same order of magnitude to findings from the TEM images. The particle diameter is an indication of the aggregation state. At lower pH more particles have aggregated. Figure 9 shows one number weighted particle size distribution of Cr_2O_3, the particle size distribution has a log-normal shape.

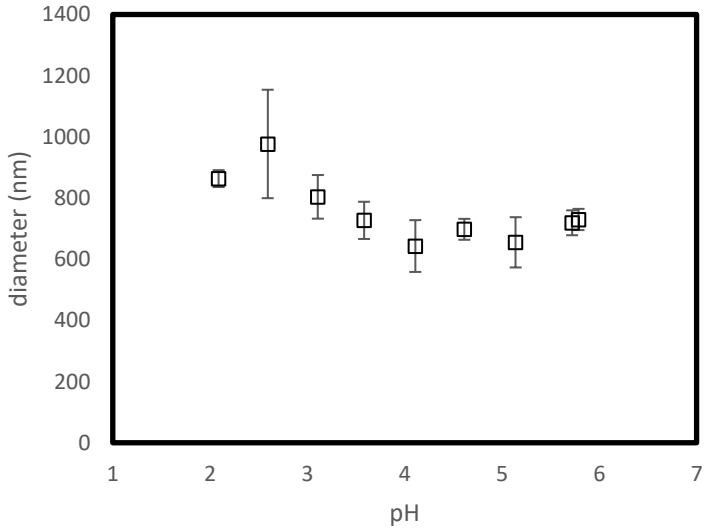

*Figure 8 DLS measurement of bare Cr2O3 (1*10-4 vf). The points shown consist of three measurements. Measurement started at pH 6*

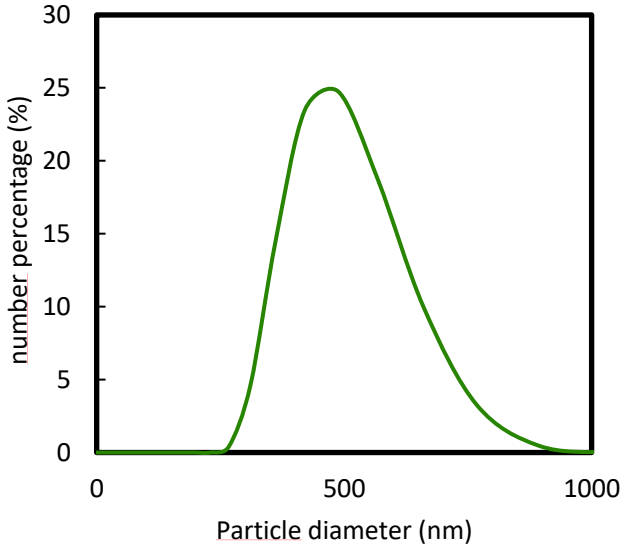

Figure 9 Number weighted PSD of bare Cr_2O_3 ($1*10^{-4}$ vf) at pH 6

4.1.c Nitrogen physisorption

Nitrogen physisorption was used to determine the total surface area of the Cr_2O_3 particles. In Figure 10 a nitrogen physisorption isotherm is shown of Cr_2O_3 particles. The BET surface area was determined to be 2.4590 ± 0.0029 m²/g. From the specific surface area, the surface area per mass, and the density of Cr_2O_3 an estimation of the average particle size can be made when the particles are assumed to be spherical. The specific surface area can be written as:

$$SSA = \frac{s}{V\rho} \tag{35}$$

with the surface area, s, is given by:

$$s = \pi d^2$$

(36)

and the volume, V, is equal to:

$$V = \frac{\pi d^3}{6}$$

(37)

Rewriting Eq. (34), the diameter of the average particle can then be calculated with:

$$d = \frac{6}{SSA\,\rho}$$

(38)

Here d is the diameter of the average particle. Assuming a density of 5.22 g/cm^3 for Cr_2O_3 [67], the average particle diameter is 470 nm, which is comparable to results gathered from DLS data. The found average particle diameter is slightly smaller than the particle radius found with DLS. Irregularly shaped particles have more surface per area per gram than spherical particles, therefore the calculated diameter of is an overestimation of the actual average diameter. In Figure 10 a small amount of hysteresis is observed, however the hysteresis is reversed to what is expected for porous materials. The desorption isotherm is below the adsorption isotherm. Capillary forces in the pores would retard the release of nitrogen molecules, therefore another effect must be responsible. We suspect either a specific interaction of the nitrogen molecules with the surface or an experimental error. That being said, the BET surface area is determined only with the adsorption isotherm and is therefore still valid.

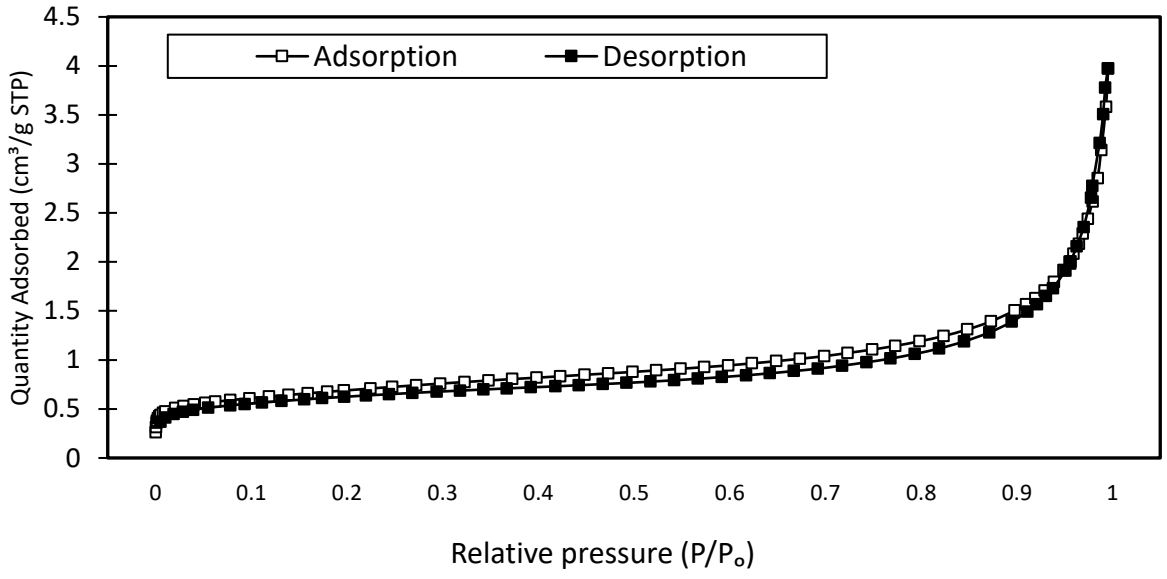

Figure 10 Nitrogen physisorption measurement of colloidal Cr_2O_3.

4.2 Zeta Potential measurements

According to our hypothesis the adsorption of proteins on surfaces is dominated by electrostatic interactions. Therefore, we need to characterize the involved surfaces charges. In Chapter 2.2.c we explained how the zeta potential can be taken as a measure of the surface charge. The zeta potential was measured through the electrophoretic mobility.

Zeta potential of Cr_2O_3, whey proteins and NaCas

The zeta potential of a dilute Cr_2O_3 ($1*10^{-4}$ vf) dispersion was measured in MilliQ. Measurement started at pH 6 and ended at pH 2. HCl and NaOH were added to change the pH and 5 measurements were performed per pH value. The average value with standard variation is shown in Figure 11. The zeta potential of a 0.1 wt% whey protein and a 0.1 wt% NaCas solution in MilliQ water was measured. Measurements started at pH 7.5 and stopped at pH 2. HCl and NaOH were again used to change the pH of the samples. Zeta potential measurements are shown in Figure 11. We find an IEP of approximately pH 4.5 for NaCas and pH 4.9 for whey proteins. This agrees with values found in the literature [35]. Both proteins have a zeta potential of approximately -40 mV at pH 7 and 30 mV at pH 3. No IEP was found for Cr_2O_3 but from extrapolating the data we expect an IEP at pH 2. The zeta potential is -10 mV at pH 3 and -40 mV at pH 7. This is comparable to the measured zeta potential of stainless steel surface in 1 mM KCl [19]. This supports the use of colloidal Cr_2O_3 as model for the surface of stainless steel. We identify two regions based on our hypothesis. Region 1 is below the IEP of the proteins, where we except maximum adsorption because the proteins are positively charged and the surface is negatively charged. At low pH the surface has almost no charge and a possibly lessened effect of the charge can be expected. In region 2, above the IEPs of the proteins, the proteins and the surface are both negatively charged and based on our hypothesis weak adsorption is expected.

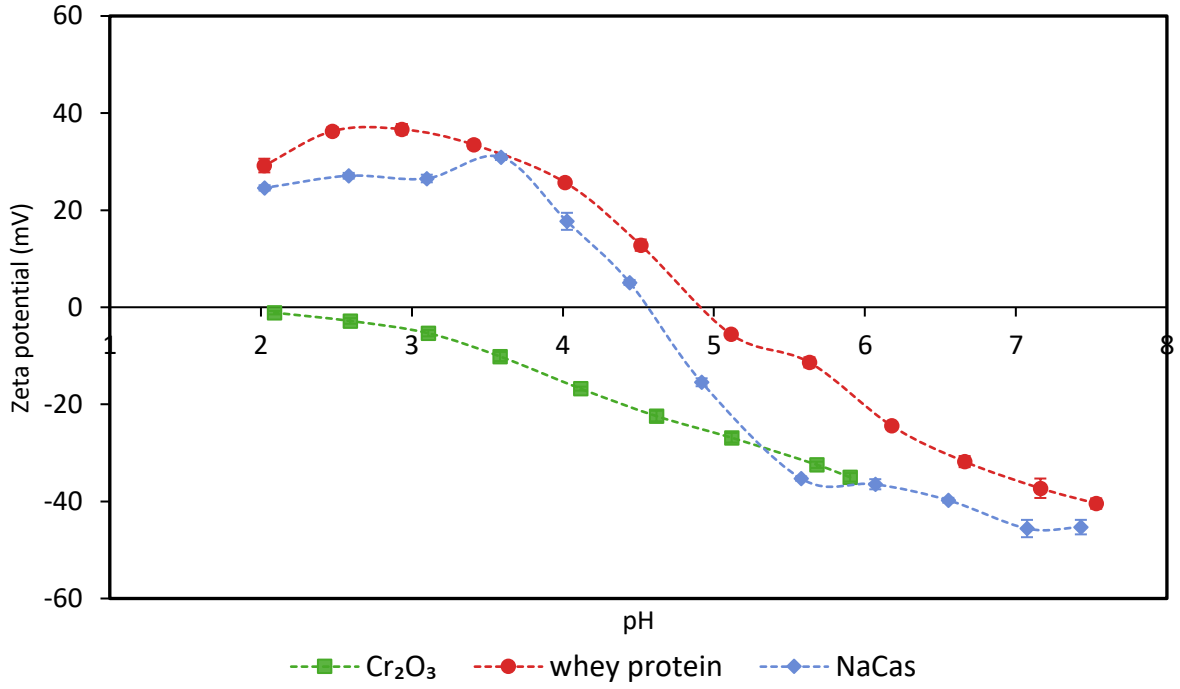

Figure 11 Zeta potential against pH for Cr_2O_3 ($1*10^{-4}$ vf), whey protein (0.1 wt%.) and NaCas (0.1 wt. Dotted lines are only there to guide the eye. Each data point is comprised of 5 measurements.

For Cr_2O_3 dispersions, the zeta potential was measured in two different environments. The experiment was repeated in a 0.1 M phosphate buffered solution. This increases the ionic strength of the solution and therefore shrinks the electric double layer of the Cr_2O_3 particles. This has an effect on the zeta potential. The zeta potential against the pH of Cr_2O_3 in MilliQ and in phosphate buffer is shown in Figure 12.

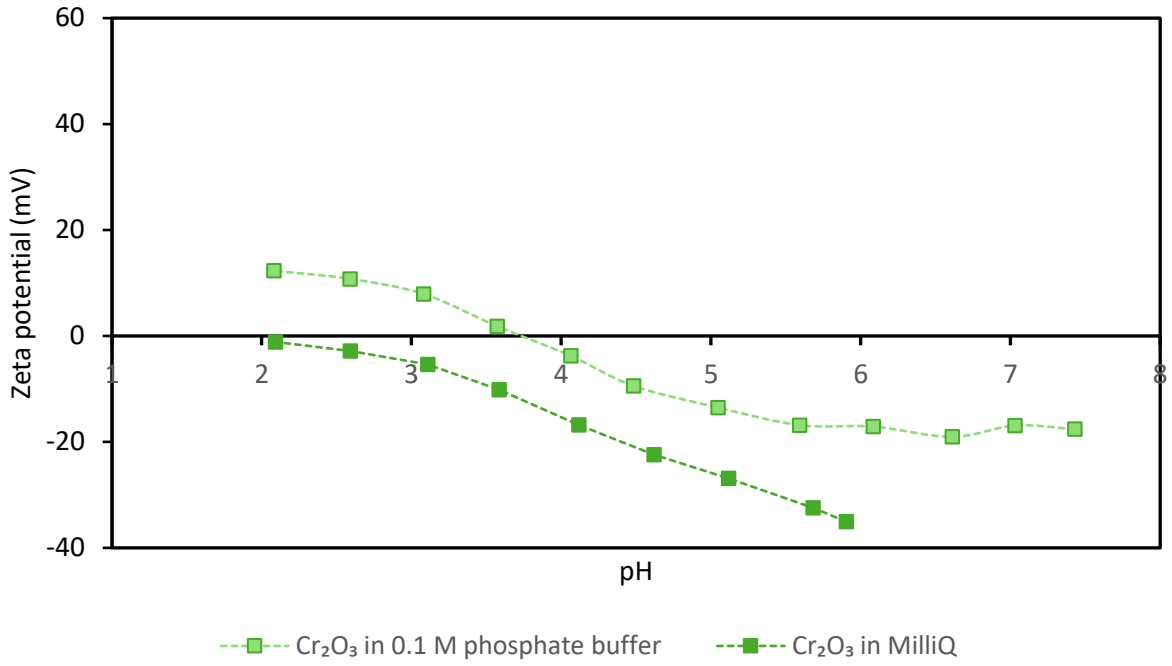

Figure 12 Zeta potential against pH for Cr_2O_3 ($1*10^{-4}$ vf) in MilliQ and Cr_2O_3 ($1*10^{-4}$ vf) in 0.1 M phosphate buffer. Dotted lines are only there to guide the eye. Each data point is comprised of 5 measurements.

The IEP of Cr_2O_3 in 0.1 M phosphate buffer is found at approximately pH 3.7. The zeta potential is increased with 15 mV for the entire pH range compared to Cr_2O_3 in MilliQ. The shape of the zeta potential plot is preserved. A change in the iconic strength of the dispersion has an effect on the zeta potential of the components but from the theory described in Chapter 2.2.c we do not expect a change in the IEP. Only a chance in the magnitude of zeta potential is expected based on Eq (6). Therefore, we suspect that a specific interaction of phosphate ions with Cr_2O_3 causes the shift in IEP. However, the regions that identified earlier in this paragraph are still valid and therefore we do not expect this change to play a significant role on the adsorption.

4.3 Colloidal stability measurements

The stability of colloidal dispersions can be characterized by the average size of the colloidal entities, relatively small in the case of separate colloidal particles, and relatively large in the case of aggregates of those same particles, resulting from poor colloidal stability. Therefore, by measuring the average colloidal size of particle or aggregates size the aggregation state of a sample can be followed. Proteins are known to have a stabilizing effect on colloidal dispersions [53]. This effect can then be used to assess the protein adsorption by studying the stabilizing effect.

4.3.a Optical microscopy

Stabilization of Cr_2O_3 dispersions were examined through optical microscopy. Visual observations showed already that the addition of protein solution to colloidal dispersions greatly increased the stability. In Figure 13 photos after vortex mixing a sample and after 30 minutes are shown.

Figure 13 Pictures of Cr_2O_3 dispersions. picture on the left is a freshly dispersed sample. Three pictures on the right show samples after 30 minutes. Sample 1 only contains Cr_2O_3 (2wt%), sample 2 contains NaCas and Cr_2O_3 (1 wt%, 2 wt%) and sample 3 contains whey proteins and Cr_2O_3 (1 wt%, 2 wt%)

In Figure 13 a completely opaque dispersions is shown as the starting condition. After 30 minutes the dispersion containing only Cr_2O_3 shows an almost completely clear supernatant and a separate sediment. Cr_2O_3 with whey protein and Cr_2O_3 with NaCas have a thinner colorless layer of fluid on top of a second a still fully opaque layer. The sample containing only Cr_2O_3 has fully sedimented after 30 minutes while the samples with added protein have not sedimented. Sedimentation of colloidal dispersions is hastened by the aggregation of the colloids. Therefore, we conclude that the addition of protein to a Cr_2O_3 halts aggregation.

Optical microscopy images were made of the previously mentioned samples. Samples containing 2 wt% Cr_2O_3 and 0.5 wt% of whey protein or NaCas are shown in Figure 14.

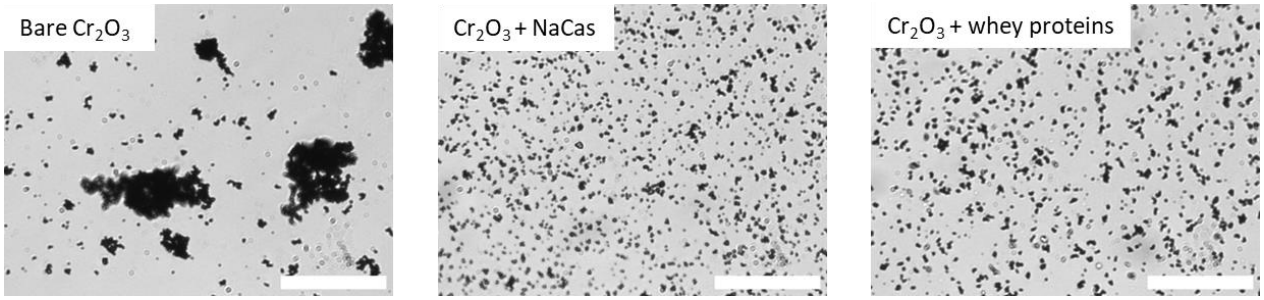

Figure 14 Optical microscope images of Cr2O3 dispersions with and without protein. The pH of dispersions is 7. Scale is bar is 50 µm.

Large aggregates are visible in samples containing only Cr_2O_3. Samples containing Cr_2O_3 and whey protein or NaCas consist of smaller aggregates. pH was 7 for all samples, showing the proteins are able to stabilize even at pH above both the IEP of protein and the IEP of Cr_2O_3.

4.3.b Analytical centrifugation

Slow analytical centrifugation was used to quantify the colloidal stability of Cr_2O_3 protein mixtures. The LUMiSizer was used to assess the stability of colloidal dispersions with added protein at different pH values. Custom Python scripts were used to analyze the LUMiSizer data. From sedimentation plots, sedimentation velocity distributions were found. These distributions were converted to hydrodynamic radii by assuming that the only forces acting on the particles are the centrifugal force and the Stokes' drag. Subsequently these distributions are fitted on a log-normal distribution in Excel. This allowed us to indicate the aggregation state with an average particle size and a standard deviation. This was done for Cr_2O_3 mixed with NaCas and

for Cr_2O_3 with whey proteins. Bare Cr_2O_3 sedimented too quickly to be analyzed with the LUMiSizer. Plots of individual distributions are included in Appendix III.

In Figure 15, particle size distribution of Cr_2O_3 stabilized with NaCas is plotted against the pH. Dispersions were made with 2 wt% and 0.5 wt% NaCas. 0.5 wt% was chosen because earlier work showed that at 0.5wt% a maximum in stabilization effect was reached. We found an average particle radius of 600 nm for particles between pH 3 and pH 6. At pH 6.5 and pH 7 the average particle radius is between 400 and 500 nm. The error bars shown indicate the width of the particle size distribution as explained in Chapter 2.3.b. The width of the particle size distribution is practically constant along the measured pH range. Compared to the particle diameter measured with DLS, which also assumes the Stokes' radius, the particles are 2 times larger than loose particles. This indicates that we are not looking at large aggregates but minimally aggregated particles. However, the DLS particle size distribution are number weighted as opposed to the transmission weighted LUMiSizer PSDs. Transmission scales with volume and volume weighted PSDs report a larger average size. This effect could contribute to found difference in size. We find no strong dependence of the particle size on the pH of NaCas covered Cr_2O_3 particles. We conclude that NaCas effectively covers Cr_2O_3 particles throughout the measured pH range and halts aggregation through adsorption.

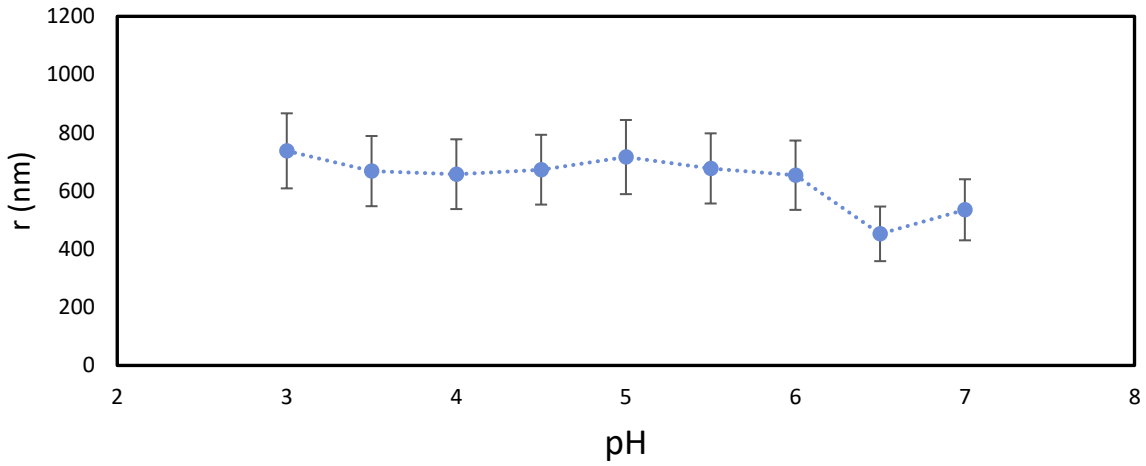

Figure 15 Average particle cluster radius against the pH. All samples contain 2 wt% Cr_2O_3 with 0.5 wt% NaCas. Error bars indicate width of the particle size distribution.

The same experiment was performed with whey protein. In Figure 16 the average found particle radius is plotted against the pH. Dispersions were made with 2 wt% Cr_2O_3 and 0.5 wt% whey protein. The average particle radius is in this instance not constant throughout the measured pH range. We find an average particle of approximately ~700 nm below pH 4 and at average particle radius of 400 nm at pH 7. The radius decreases gradually between pH 7 and pH 3. The standard deviation is nearly constant. The samples are as polydisperse at all measured pH points. The higher average particle radius found at low pH indicates that there are aggregated particles. The adsorption of protein halts aggregation, therefore we deduce that less adsorption happens at lower pH. At pH 7 a small average particle radius is found, indicating sufficient adsorption of whey protein to stabilize the Cr_2O_3 dispersions. Nevertheless, even though at pH 7 both the whey protein and the Cr_2O_3 have a negative zeta potential. The rise in average particle size at low pH can also be explained by the lower zeta potential of Cr_2O_3. Colloidal dispersions are unstable if the colloids have a low zeta potential [44].

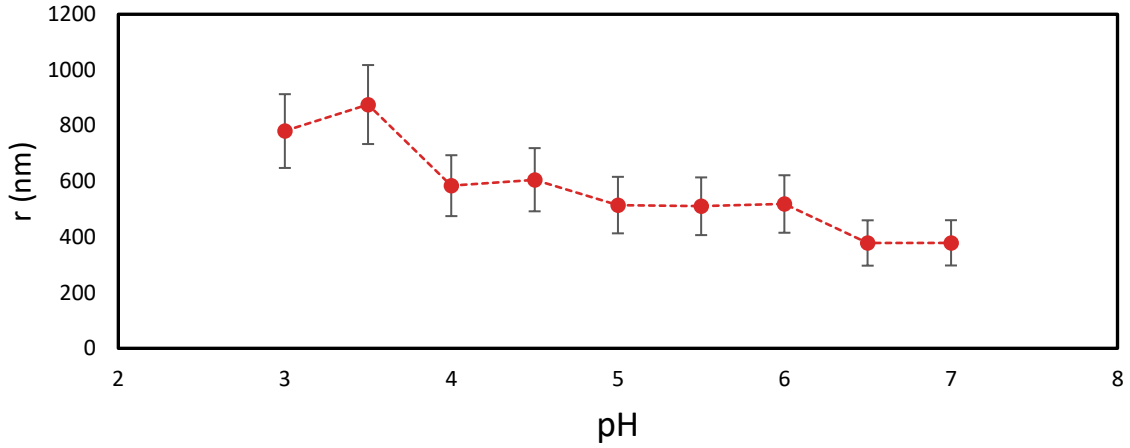

Figure 16 Average particle cluster radius against the pH. All samples contain 2 wt% Cr_2O_3 with 0.5 wt% whey protein. Error bars indicate the width of the particle size distribution.

4.4 Adsorption isotherms

Adsorption isotherms were measured of NaCas and whey protein on Cr_2O_3 at 20 °C. The amount of protein in solution was measured and compared to the amount of added protein to determine the adsorbed amount. The concentration was determined through UV-Vis spectroscopy. The Cr_2O_3 powder was found to be contaminated with Cr(VI). Cr(VI) is present at low concentration and normal pH ([Cr] < 1mM, 3 < pH) as two hydration forms, $HCrO_4^-$ and CrO_4^{2-} which both strongly absorb light in the UV-Vis region[65], [66]. In Appendix I is explained how we filter out the absorption by contaminants with custom Python scripts based on a classical least squares method.

4.4.a Adsorption isotherms of NaCas onto Cr_2O_3

The adsorption of NaCas on Cr_2O_3 was measured at 20 °C at pH 3, pH 5 and pH 7 and is presented in Figure 17. Substantial adsorption was found at all three pH values. A maximum adsorption of ~3 mg/m^2 was reached at a free protein concentration of roughly 200 mg/L for all samples. A Langmuir type isotherm was fitted on the adsorption data. With an assumed irreversible adsorbed amount of 1.5 mg/m^2 and an equilibrium constant, k_{eq}, of 1700 M^{-1}, represented by the dotted line in Figure 17**.** Fit of the Langmuir adsorption isotherms is not good enough to put physical meaning to the equilibrium constant. In addition the equilibrium constant would only provide meaningful insights if all conditions for the Langmuir isotherms were met as explained by Latour [68]. The maximum adsorbed amount corresponds to one monolayer of sodium caseinates. We confirmed this with following rough calculation. We assume an average weight of 22.9 kDa based on the weights on the individual caseins and their prevalence [35]. For the radius we use that α and β caseins have a hydrodynamic radius between 2.9 nm and 3.9 nm depending on the pH[69]. Moreover, we assume an assumed approximate hydrodynamic radius of 1.8 nm [70]and HCC packing, which has a 2D packing efficiency of 90.64%, and an average weight of 22.9 kDa. The amount adsorbed in g/m^2 is calculated with:

$$q = \frac{s * PE}{\pi r^2} * m \qquad (39)$$

Here s is the surface and is set at 1 m^2, PE is the packing efficiency, r is the radius of the protein and m the mass per protein. We find an expected monolayer of ~3.4 mg/m^2. Considering the assumptions made, this is in good agreement with the found value of ~3 mg/m^2. Furthermore, no effect of the pH on the adsorption isotherms was observed. Which means adsorption occurs even when the zeta potential measurements indicate that the sign of the charge on the surface is the same. We address the implications of these findings in the discussion in more detail.

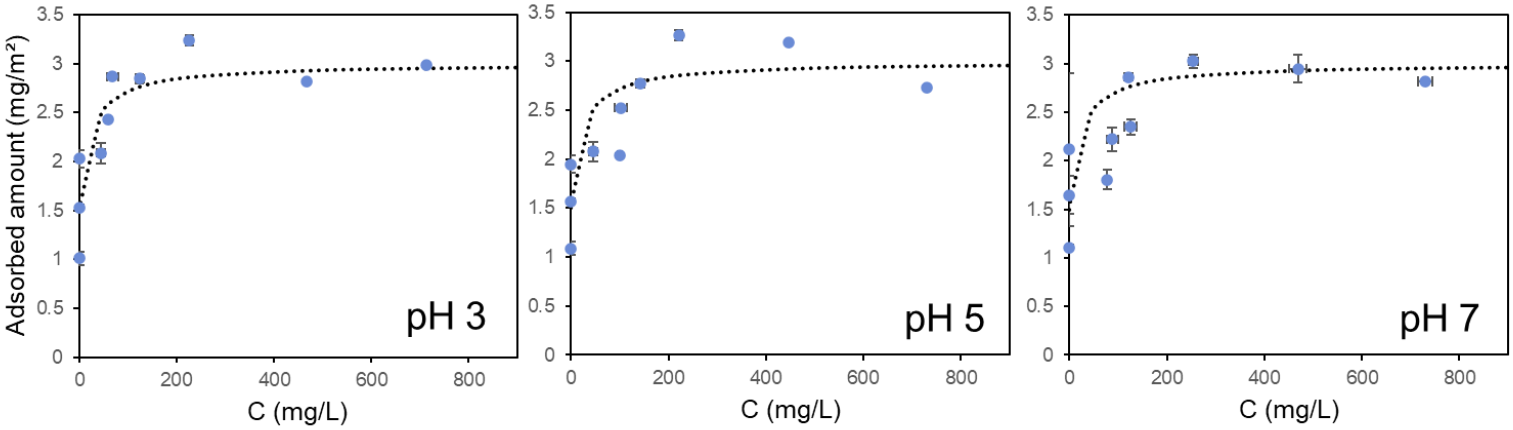

Figure 17 Adsorption isotherms of NaCas onto Cr_2O_3. Adsorbed amount against the steady state protein concentration. The dotted lines represent a Langmuir type adsorption isotherm with an assumed irreversible adsorbed 1.5 mg/m^2 of NaCas. Measured at pH 3, 5, and 7. T = 20 °C

4.4.b Adsorption isotherms of whey proteins on Cr_2O_3

The adsorption of whey proteins was measured at pH 3, pH 5 and pH 7 at 20 °C. In Figure 18 the adsorption isotherms are shown. Absorption at pH 5 and pH 7 is strong and reaches a maximum after at a free protein concentration of ~100 mg/L. Maximum adsorption is approximately 2.5 mg/m^2. Adsorption at pH 3 does

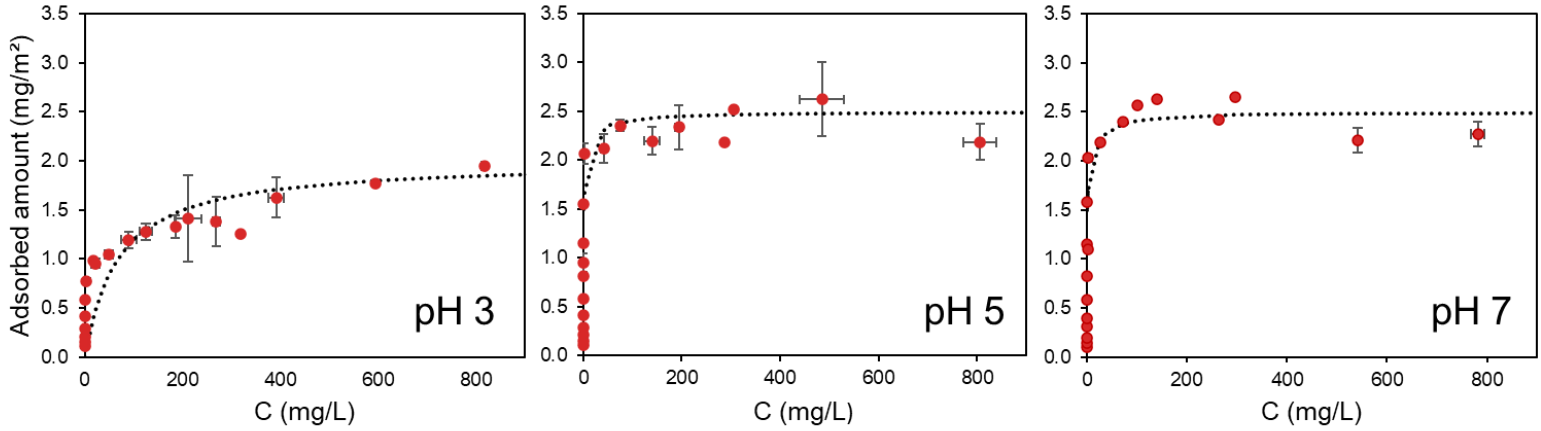

Figure 18 Adsorption isotherms of whey proteins onto Cr_2O_3. Adsorbed amount against the steady state protein concentration. The dotted lines represent a Langmuir type adsorption isotherm. For pH 5 and pH 7 with an assumed irreversible adsorbed 1.5 mg/m2 of NaCas. Measured at pH 3, 5, and 7. T = °20 C

not reach a maximum in the studied protein concentration range. The dotted lines are Langmuir type isotherms, where for pH 5 and pH 7 an irreversible adsorbed of 1.5 mg/m^2 was assumed and an equilibrium constant of, k_{eq}, of 1700 M^{-1}. For pH 3 the dotted line is a Langmuir isotherm with no assumed irreversible adsorption and an equilibrium constant of 150 M^{-1}. The maximum adsorption of 2.5 mg/m^2 corresponds to one monolayer according to calculations done by Wahlgren et al. where they calculate that a HCC packed

monolayer of pure β-lactoglobulin is 2.7 mg/m^2 [21]. We find identical adsorption behavior at pH 5 and pH 7, even though we know from zeta potential measurements that the surface charge of whey proteins Is strongly negative at pH 7 and close to neutral at pH 5 while the surface is strongly negatively charged at both pH. We therefore have adsorption regardless of the same sign surface charge. At pH 3 we expect stronger adsorption based on the surface charge; however, the opposite is observed. β-lactoglobulin, the main constituent of whey protein, is present as a dimer or as monomer depending on the pH. α-lactalbumin is a monomer at all measured pH values. At low pH the monomer of β-lactoglobulin is more prevalent than the dimer [34]. The monomer packing is less efficient than the dimer packing on the surface assuming that proteins arrive randomly and subsequentially at the surface. Monomers exclude more surface than dimers. This gives an explanation to the found lower adsorption at pH 3.

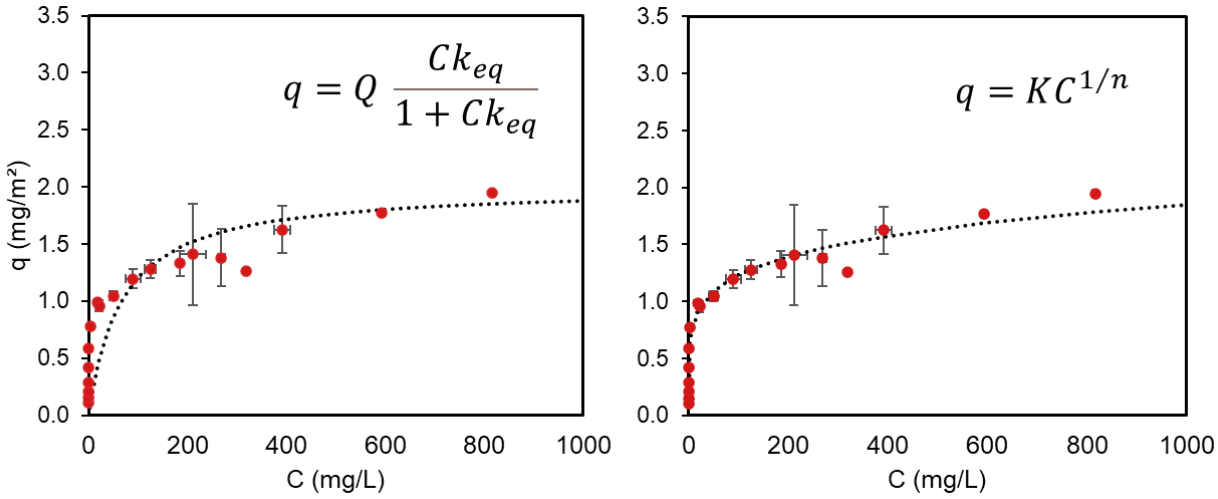

Figure 19 Adsorption of whey protein at pH 3 on Cr2O3. In the left figure the dotted line represents a Langmuir isotherm. In the right figure the dotted line represents a Freundlich isotherm. T = 20 °C

In Figure 19 the adsorption of whey protein at pH 3 is shown again. This time two different isotherms are used to fit the adsorption data. The figure on the left uses the Langmuir adsorption isotherm while the figure in the right uses a Freundlich isotherm. The data points show a large deviation from the fitted isotherm for the Langmuir isotherm, but they are however fitted with great accuracy on the Freundlich isotherm. As explained in Chapter 2.1.b Langmuir type isotherms can only be properly applied when the conditions on which the theoretical model is based are met. In our hypothesis we state that we expect that electrostatic interactions play an important role in the adsorption of proteins on a surface. This *a priori* rules out Langmuir type adsorption. The adsorption sites are not identical due to the lateral electrostatic interaction with already adsorbed proteins. This means that the previously mentioned equilibrium constant found by fitting Langmuir isotherms does not hold a physical meaning apart from fitting a curve on the data. With a low equilibrium constant, the deviation from Langmuir type adsorption becomes clear. Freundlich type adsorption assumes heterogenous adsorption sites, which concurs with our molecular picture. Adsorbed proteins influence the adsorption energy of the next protein that adsorbs. Which makes the Freundlich isotherm more suited to fit our data. However, as mentioned in Chapter 2.1.b the equilibrium constant, K, and the correction factor, n, only have an empirical basis. Therefore, the Freundlich isotherms only confirms our suspicions that we are dealing with heterogenous adsorption sites, but the equilibrium constants lack a physical meaning because the Freundlich isotherm is not based on physical model.

4.4.c Reversibility of adsorption

The reversibility of adsorption of NaCas and of whey proteins onto Cr_2O_3 was tested by washing dispersions of Cr_2O_3 with adsorbed protein with fresh MilliQ water at pH 7 and analyzing the protein content in the runoff. Three washes were performed, one after an hour, another after two hour and a final wash after waiting overnight. The reversibility of adsorption is shown in Figure 20, the amount of protein is normalized to adsorbed amount on the surface before washing.

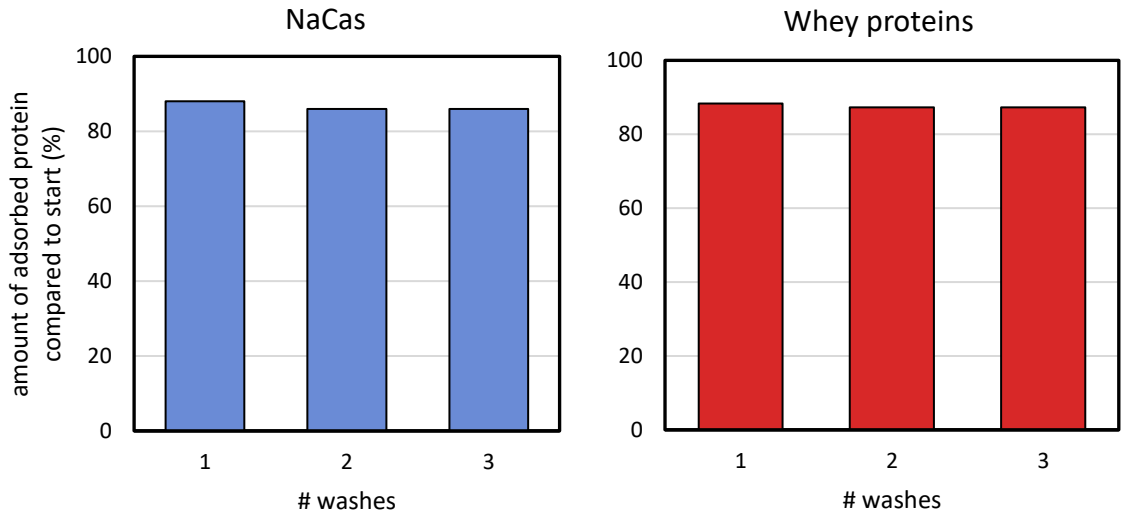

Figure 20 Reversibility of adsorption. The amount of protein on the surface of the Cr_2O_3 compared to unwashed particles. 1st wash is after one hour, 2nd wash is after another hour and 3rd wash is after soaking overnight.

For NaCas we find that after washing once with MilliQ water pH 7, 12% of the NaCas is removed. Subsequent washing removes another 2%, the third wash removes no measurable amount of protein. For whey protein the first wash removes 12% of the adsorbed protein, the second wash removes another 1 %, and the third wash does not remove a measurable amount of protein. For both Cr_2O_3 protein mixtures almost 90% of the protein was found to be irreversible adsorbed onto the surface of Cr_2O_3. The irreversibility of the adsorption is thought to be due to the high adsorption energy and reorientation of the proteins on the surface[16], [71]. This is line in with our finding of a rapid formation of a monolayer on the surface, indicating a high adsorption energy. Furthermore, the irreversibility of the adsorption also validates our suspicion that a Langmuir type isotherm, although often used for protein adsorption, is not suited to describe the adsorption behavior of NaCas and whey protein onto Cr_2O_3. To accurately describe adsorption with Langmuir type isotherm the adsorption must be reversible.

4.5 Discussion

This research was prompted by earlier work on the pH dependence of the fouling of milk proteins on stainless steel surfaces. In relevant conditions, 90 °C 2 wt% protein, fouling was found to be maximal between pH 4 and pH 5. Zeta potential measurement confirmed that is the region where the signs of the surface charge are opposite, with a negatively charged surface and positively charged proteins. Leading to the hypothesis that electrostatic interactions dominate the adsorption behaviors of NaCas and whey proteins onto stainless steel surfaces. However, for NaCas no pH dependence was found in colloidal stability measurements and no pH dependence was found on the adsorption measured through UV-Vis spectroscopy. Similar finds were made for the adsorption behavior of whey proteins, only lessened adsorption was found at low pH. Our hypothesis in combination with the measured zeta potentials predicted a maximum

adsorption between the IEP of the protein and IEP of Cr2O3. No such maximum was not found for either NaCas or whey proteins.

We have identified strong adsorption in pH regions where because of the overall surface charge we would not expect this. Therefore, we conclude that the adsorption behavior of whey protein and NaCas is not dominated by electrostatic interactions. Other explanations are necessary to rationalize the observed adsorption behavior. Earlier works on the adsorption of β-lactoglobulin have already determined that adsorption is found on surface with same sign of charge [21], [23], [72]. They noted that the charge distribution is not uniform on the surface of a protein. On β-lactoglobulin at pH 7, although the zeta potential is negative, there are positively charged regions [23]. Globular proteins commonly have regions with different charges [28]. Unfolded proteins such as caseins possess differently charged residues as well [18]. Because the proteins are in solution, they are able to freely rotate. Our new hypothesis then is that proteins reorient themselves in space to minimize the electrostatic repulsion with the surface for same sign adsorption. Schematically drawn in Figure 21 for whey proteins and NaCas in Figure 21.

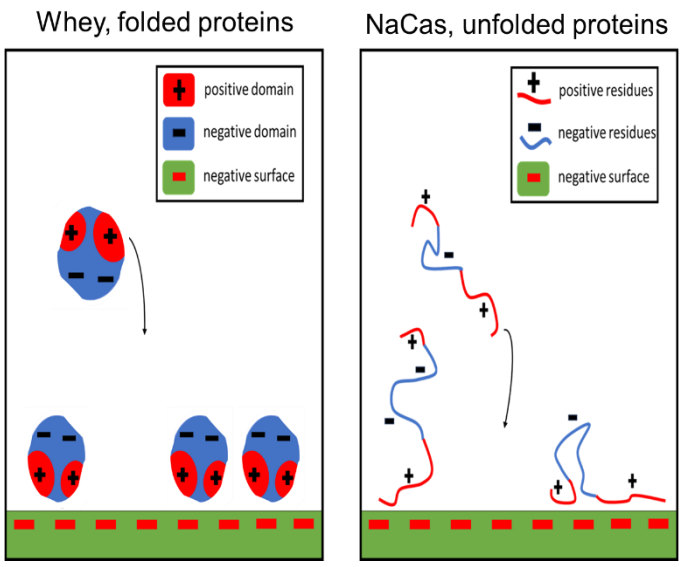

Figure 21 Schematic drawing of how proteins reorient themselves to minimize electrostatic repulsions on a surface with same sign of charge.

If the reorienting of proteins to minimize/maximize electrostatic interactions were the only reason for the adsorption we would still expect an effect of the pH. Therefore, the driving force is then not the electrostatic attraction between the surface and the protein but hydrophobic interactions with the solvent [16] and the Van der Waals interaction with the surface. Which can be expected because of the hydrophobic nature of NaCas [18] and the strong Van der Waals interactions with Cr_2O_3 discussed in Chapter 2.2.b. Furthermore, simulations for adsorption of β-lactoglobulin onto gold surfaces at low pH showed Van der Waals forces caused the adsorption [73]. Explaining the pH independent formation of a monolayer. The weaker adsorption of whey protein is then not explained by a difference in zeta potential but is caused by the presence of β-lactoglobulin monomers at low pH.

This research was performed on two types of milk proteins. We think these results can generalized to a larger class of proteins. The description of the adsorption behavior of whey proteins and NaCas is not unique to these specific proteins. In the introduction the importance of the protein transition was stressed. We expect plant-based globular proteins or unfolded proteins to show the same type of behavior. However, protein remain a complex class of molecules and it is thus difficult to make predictions.

5. Conclusion and Outlook

The role of electrostatic interactions in the adsorption of whey proteins and NaCas onto colloidal Cr_2O_3 has been investigated through measuring the change in colloidal stability and through the construction of adsorption isotherms at 20 °C. Via zeta potential measurements of IEP ~2 pH for Cr_2O_3, 4.6 pH for NaCas and 4.9 pH for whey proteins. Maximum adsorption between the IEPs of the protein and Cr_2O_3 was expected, where the sign of charge is opposite. Experiments showed that adsorption of protein was not dependent on the pH.

For NaCas, the adsorption and resulting stabilizing properties were not found to be dependent on the pH. Between pH 3 to pH 7 a monolayer of protein was adsorbed. The monolayer was found to be approximately 90% irreversibly bound to surface. Strong adsorption of NaCas onto Cr_2O_3 was found even when the zeta potential indicates the same sign of surface charge. Therefore, we conclude that the adsorption of NaCas is not dominated by electrostatic interactions.

In the case of whey protein, the adsorption and resulting stabilizing properties were found to be less at low pH. Adsorption isotherms showed that a monolayer of whey protein adsorbed at pH 5 and pH 7 whereas at pH 3 adsorption was weaker. We explain this difference by the presence of β-lactoglobulin monomers at pH 3 and dimers at higher pH. Monomers have a less efficient packing, explaining the lessened adsorption. The main conclusion is once again that electrostatic interactions are not the dominant factor in adsorption.

We hypothesize that electrostatic repulsions between the negatively charged surface of colloidal Cr_2O_3 and the overall negative surface charge of protein above IEP are minimized by the ability of proteins to direct positively charged or neutral regions to the surface. The driving force of protein adsorption is then not electrostatic attraction but hydrophobic interactions.

In future research, the hypothesis of protein reorientation might be validated with circular dichroism spectroscopy [74]. If our hypothesis is correct, the orientation of adsorbed protein on the surface should differ above and below the IEP. Another suggestion for future work is to vary the ionic strength. In this research experiments have been conducted in mostly MilliQ water with added HCl and NaOH to change the pH. In phosphate buffers, different IEP were found, although it is not clear whether this was due to the higher ionic strength of specific adsorption of phosphate ions. Lastly, in the introduction the relevance of this research was said to not only be for cow's milk but also for plant-based milks. Our findings on the adsorption of milk proteins on Cr_2O_3 give strong indications that non-milk proteins are expected to show similar behavior, but it would be informative to study these.

Acknowledgments

To start, I want to thank Ben for his supervision. This project would not haven been possible without your ideas and knowledge. Your door was always open for a quick question or an impromptu in-depth discussion. I am really grateful that you gave me the opportunity to learn Python for this project. Your enthusiasm for Python was contagious and I really enjoyed writing code to solve the problems that we encountered in the lab. Next I would like to thank Hans for the discussions on Friday. Without your extensive knowledge on all things fouling and proteins we would have been lost. I also would like to thank Dominique for helping me with the TEM and also for providing a very nice lab environment. Not only during my Master's thesis but during my Bachelor's as well. For their help with my project I would like to thank Juliette Verschoor (MCC) for performing the nitrogen physisorption measurements and Petra de Jongh (MCC) for allowing us to do the nitrogen physisorption measurements. Lastly, I would like to thank all the students and staff at FCC for providing a very nice working environment this last year. You made studying and researching at FCC a really great experience.

Bibliography

[1] D. I. Wilson, "Fouling during food processing – progress in tackling this inconvenient truth," *Curr Opin Food Sci*, vol. 23, pp. 105–112, Oct. 2018, doi: 10.1016/J.COFS.2018.10.002.

[2] T. Huppertz and H. Nieuwenhuijse, "Constituent fouling during heat treatment of milk: A review," *International Dairy Journal*, vol. 126. Elsevier Ltd, Mar. 01, 2022. doi: 10.1016/j.idairyj.2021.105236.

[3] E. Sadeghinezhad, S. N. Kazi, A. Badarudin, M. N. M. Zubair, B. L. Dehkordi, and C. S. Oon, "A review of milk fouling on heat exchanger surfaces," *Reviews in Chemical Engineering*, vol. 29, no. 3, pp. 169–188, Jun. 2013, doi: 10.1515/REVCE-2013-0003.

[4] H. Müller-Steinhagen, M. R. Malayeri, and A. P. Watkinson, "Heat Exchanger Fouling: Mitigation and Cleaning Strategies," *http://dx.doi.org/10.1080/01457632.2010.503108*, vol. 32, no. 3–4, pp. 189–196, Mar. 2011, doi: 10.1080/01457632.2010.503108.

[5] M. Mauermann, U. Eschenhagen, T. Bley, and J. P. Majschak, "Surface modifications – Application potential for the reduction of cleaning costs in the food processing industry," *Trends Food Sci Technol*, vol. 20, no. SUPPL. 1, pp. S9–S15, Jan. 2009, doi: 10.1016/J.TIFS.2009.01.020.

[6] A. J. Van Asselt, M. M. M. Vissers, F. Smit, and P. De Jong, "In-line control of fouling," in *Proceedings of Heat Exchanger Fouling and Cleaning - Challenges and Opportunities*, H. Muller-Steinhagen, Ed., Kloster Irsee: Curian Associates Inc., Jun. 2005.

[7] B. P. Ismail, L. Senaratne-Lenagala, A. Stube, and A. Brackenridge, "Protein demand: review of plant and animal proteins used in alternative protein product development and production," vol. 10, no. 4, 2020, doi: 10.1093/af/vfaa040.

[8] S. Roe *et al.*, "Contribution of the land sector to a 1.5 °C world," *Nature Climate Change*, vol. 9, no. 11. Nature Publishing Group, pp. 817–828, Nov. 01, 2019. doi: 10.1038/s41558-019-0591-9.

[9] J. Wang, L. Li, N. Fu, R. Mercade-Prieto, and X. D. Chen, "A Comparative Study on Fouling and Cleaning Characteristics of Soy Protein Isolate (SPI)," *International Journal of Food Engineering*, vol. 14, no. 4, Apr. 2018, doi: 10.1515/IJFE-2017-0381/MACHINEREADABLECITATION/RIS.

[10] R. Kamath, R. Jimenez-Flores, and D. R. Heldman, "Investigation of Blended Milk-Pea Protein Beverage Fouling and Cleaning Using a Quartz Crystal Microbalance with Dissipation," *ACS Food Science & Technology*, Dec. 2023, doi: 10.1021/ACSFOODSCITECH.3C00347.

[11] R. Chan and V. Chen, "Characterization of protein fouling on membranes: opportunities and challenges," *J Memb Sci*, vol. 242, pp. 169–188, 2004, doi: 10.1016/j.memsci.2004.01.029.

[12] T. K. Tuoc, "Fouling in Dairy Processes," in *Mineral Scales and Deposits: Scientific and Technological Approaches*, Elsevier Inc., 2015, pp. 533–556. doi: 10.1016/B978-0-444-63228-9.00020-6.

[13] Tromp Hans, "Personal Communication." 2023.

[14] M. Mozetič, A. Vesel, J. Kovač, R. Zaplotnik, M. Modic, and M. Balat-Pichelin, "Formation and reduction of thin oxide films on a stainless steel surface upon subsequent treatments with oxygen and hydrogen plasma," *Thin Solid Films*, vol. 591, pp. 186–193, Sep. 2015, doi: 10.1016/J.TSF.2015.02.007.

[15] Jeurnink T.J.M, P. Walstra, and C. G. De Kruif, "Mechanisms of fouling in dairy processing," *Neth Milk Dairy J*, pp. 407–426, 1996.

[16] M. Rabe, D. Verdes, and S. Seeger, “Understanding protein adsorption phenomena at solid surfaces,” *Advances in Colloid and Interface Science*, vol. 162, no. 1–2. Elsevier B.V., pp. 87–106, Feb. 17, 2011. doi: 10.1016/j.cis.2010.12.007.

[17] H. Tamura, K. Mita, A. Tanaka, and M. Ito, “Mechanism of Hydroxylation of Metal Oxide Surfaces,” *J Colloid Interface Sci*, vol. 243, no. 1, pp. 202–207, Nov. 2001, doi: 10.1006/JCIS.2001.7864.

[18] P. F. Fox, T. Uniacke-Lowe, P. L. H. McSweeney, and J. A. O’Mahony, “Dairy chemistry and biochemistry, second edition,” *Dairy Chemistry and Biochemistry, Second Edition*, pp. 1–584, Jan. 2015, doi: 10.1007/978-3-319-14892-2/COVER.

[19] Y. Hedberg, X. Wang, J. Hedberg, M. Lundin, E. Blomberg, and I. Odnevall Wallinder, “Surface-protein interactions on different stainless steel grades: Effects of protein adsorption, surface changes and metal release,” *J Mater Sci Mater Med*, vol. 24, no. 4, pp. 1015–1033, Apr. 2013, doi: 10.1007/S10856-013-4859-8.

[20] S. Demanèche, J.-P. Chapel, L. J. Monrozier, and H. Quiquampoix, “Dissimilar pH-dependent adsorption features of bovine serum albumin and-chymotrypsin on mica probed by AFM,” *Colloids Surf B Biointerfaces*, vol. 70, pp. 226–231, 2009, doi: 10.1016/j.colsurfb.2008.12.036.

[21] M. Wahlgren and T. Arnebrant, “Adsorption of β-Lactoglobulin onto silica, methylated silica, and polysulfone,” *J Colloid Interface Sci*, vol. 136, no. 1, pp. 259–265, Apr. 1990, doi: 10.1016/0021-9797(90)90096-7.

[22] H. Swenson and N. P. Stadie, “Langmuir’s Theory of Adsorption: A Centennial Review,” *Langmuir*, 2019, doi: 10.1021/ACS.LANGMUIR.9B00154/ASSET/IMAGES/LARGE/LA-2019-00154A_0009.JPEG.

[23] J. Saikia, B. Saha, and G. Das, “Interpreting the adsorption of serum albumin and lactoglobulin onto ZnS nanopaticles: Effect of conformational rigidity of the proteins,” *J Colloid Interface Sci*, vol. 416, pp. 235–242, Feb. 2014, doi: 10.1016/J.JCIS.2013.10.053.

[24] I. Langmuir, “THE ADSORPTION OF GASES ON PLANE SURFACES OF GLASS, MICA AND PLATINUM.,” *J Am Chem Soc*, vol. 40, no. 9, pp. 1361–1403, Sep. 1918, doi: 10.1021/ja02242a004.

[25] M. Ozboyaci, D. B. Kokh, S. Corni, and R. C. Wade, “Modeling and simulation of protein-surface interactions: Achievements and challenges,” *Q Rev Biophys*, vol. 49, Jan. 2016, doi: 10.1017/S0033583515000256.

[26] H.-X. Zhou and X. Pang, “Electrostatic Interactions in Protein Structure, Folding, Binding, and Condensation Graphical Abstract HHS Public Access,” *Chem Rev*, vol. 118, no. 4, pp. 1691–1741, 2018, doi: 10.1021/acs.chemrev.7b00305.

[27] X.-J. Zhang, “Van der Waals Forces,” in *Encyclopedia of Tribology*, Boston, MA: Springer US, 2013, pp. 3945–3947. doi: 10.1007/978-0-387-92897-5_457.

[28] D. J. Barlow and J. M. Thornton, “The distribution of charged groups in proteins,” *Biopolymers*, vol. 25, no. 9, pp. 1717–1733, Sep. 1986, doi: 10.1002/BIP.360250913.

[29] S. Kalam, S. A. Abu-Khamsin, M. S. Kamal, and S. Patil, “Surfactant Adsorption Isotherms: A Review,” *ACS Omega*, vol. 6, no. 48, p. 32342, Dec. 2021, doi: 10.1021/ACSOMEGA.1C04661.

[30] T. C. Krishna *et al.*, “Influence of ultra-heat treatment on properties of milk proteins,” *Polymers (Basel)*, vol. 13, no. 18, Sep. 2021, doi: 10.3390/POLYM13183164.

[31] A. A. Morgan and E. Rubenstein, “Proline: The Distribution, Frequency, Positioning, and Common Functional Roles of Proline and Polyproline Sequences in the Human Proteome,” *PLoS One*, vol. 8, no. 1, p. e53785, Jan. 2013, doi: 10.1371/JOURNAL.PONE.0053785.

[32] M. Boland, “Whey proteins,” in *Handbook of Food Proteins*, Cambridge: Woodhead Publishing, 2011, pp. 30–55.

[33] E. A. Permyakov and L. J. Berliner, “α-lactalbumin: structure and function,” *FEBS lett.*, 2000, doi: 10.1016/S0014-5793(00)01546-5.

[34] L. Da Rocha, A. M. Baptista, and S. R. R. Campos, “Approach to Study pH-Dependent Protein Association Using Constant-pH Molecular Dynamics: Application to the Dimerization of β-Lactoglobulin,” *Cite This: J. Chem. Theory Comput*, vol. 18, 2022, doi: 10.1021/acs.jctc.1c01187.

[35] W. N. Eigel *et al.*, “Nomenclature of Proteins of Cow’s Milk: Fifth Revision,” *J Dairy Sci*, vol. 67, no. 8, pp. 1599–1631, 1984, doi: 10.3168/jds.S0022-0302(84)81485-X.

[36] T. C. Krishna *et al.*, “Influence of ultra-heat treatment on properties of milk proteins,” *Polymers*, vol. 13, no. 18. MDPI, Sep. 01, 2021. doi: 10.3390/polym13183164.

[37] M. M. Abdullah, F. M. Rajab, and S. M. Al-Abbas, “Structural and optical characterization of Cr2O3 nanostructures: Evaluation of its dielectric properties,” *AIP Adv*, vol. 4, no. 2, p. 27121, Feb. 2014, doi: 10.1063/1.4867012/20040.

[38] A. Kumar, F. Ropital, T. de Bruin, and B. Diawara, “Effects of surface orientations of Cr2O3 on CO2 adsorption: A DFT approach,” *Appl Surf Sci*, vol. 529, p. 147127, Nov. 2020, doi: 10.1016/J.APSUSC.2020.147127.

[39] P. H. Fang and W. S. Brower, “Dielectric Constant of Cr2O3 Crystals,” 1963.

[40] C. G. Malmberg and A. A. Maryott, “Dielectric Constant of Water from 0 0 to 100 0 C,” *J Res Natl Bur Stand (1934)*, vol. 56, no. I, 1956.

[41] E. M. Lifshitz, “The Theory of Molecular Attractive Forces between Solids ,” *J. Exper. Theoret, Phys. USSR*, vol. 2, no. 1, Jan. 1954.

[42] D. Cappus *et al.*, “Hydroxyl groups on oxide surfaces: NiO(100), NiO(111) and Cr2O3(111),” *Chem Phys*, vol. 177, no. 2, pp. 533–546, Nov. 1993, doi: 10.1016/0301-0104(93)80031-4.

[43] D. H. Everett, *Basic Principles of Colloid Science*. London: The Royal Society of Chemistry , 1988.

[44] D. J. Pochapski, C. Carvalho, D. Santos, G. W. Leite, S. H. Pulcinelli, and C. V. Santilli, “Zeta Potential and Colloidal Stability Predictions for Inorganic Nanoparticle Dispersions: Effects of Experimental Conditions and Electrokinetic Models on the Interpretation of Results,” vol. 10, p. 33, 2022, doi: 10.1021/acs.langmuir.1c02056.

[45] J. M. Berg, A. Romoser, N. Banerjee, R. Zebda, and C. M. Sayes, “The relationship between pH and zeta potential of ∼ 30 nm metal oxide nanoparticle suspensions relevant to in vitro toxicological evaluations,” *http://dx.doi.org/10.3109/17435390903276941*, vol. 3, no. 4, pp. 276–283, 2009, doi: 10.3109/17435390903276941.

[46] V. Agmo Hernández, “An overview of surface forces and the DLVO theory,” *ChemTexts*, vol. 9, no. 4, pp. 1–16, Dec. 2023, doi: 10.1007/S40828-023-00182-9/FIGURES/17.

[47] P. Atkins, *Physical Chemistry*, 11th ed. Oxford University Press, 2018.

[48] S. Brunauer, P. H. Emmett, and E. Teller, “Adsorption of Gases in Multimolecular Layers,” 1938, Accessed: Jan. 25, 2024. [Online]. Available: https://pubs.acs.org/sharingguidelines

[49] P. De Jongh and J. Verschoor, *Course manual “Physisorption” Advanced Catalysis*. 2023.

[50] K. L. Planken, B. W. M. Kuipers, and A. P. Philipse, “Model Independent Determination of Colloidal Silica Size Distributions via Analytical Ultracentrifugation,” *Anal. Chem*, vol. 80, no. 23, p. 25, 2008, doi: 10.1021/ac801556t.

[51] H. Chen, X. Jia, M. Fairweather, and T. N. Hunter, “Characterising the sedimentation of bidisperse colloidal silica using analytical centrifugation,” *Advanced Powder Technology*, vol. 34, no. 2, p. 103950, Feb. 2023, doi: 10.1016/J.APT.2023.103950.

[52] B. J. Lee, M. Fettweis, E. Toorman, and F. J. Molz, “Multimodality of a particle size distribution of cohesive suspended particulate matters in a coastal zone,” *J Geophys Res Oceans*, vol. 117, no. C3, p. 3014, Mar. 2012, doi: 10.1029/2011JC007552.

[53] Á. González García, M. M. B. Nagelkerke, R. Tuinier, and M. Vis, “Historical Perspective Polymer-mediated colloidal stability: on the transition between adsorption and depletion,” 2019, doi: 10.1016/j.cis.2019.102077.

[54] G. G. Stokes, “ON THE EFFECT OF THE INTERNAL FRICTION OF FLUIDS ON THE MOTION OF PENDULUMS,” *Transactions of the Cambridge Philosophical Society*, vol. 3, pp. 1880–1905.

[55] J. C. Thomas, “The determination of log normal particle size distributions by dynamic light scattering,” *J Colloid Interface Sci*, vol. 117, no. 1, pp. 187–192, May 1987, doi: 10.1016/0021-9797(87)90182-2.

[56] “Log-normal Distribution - A simple explanation | by Maja Pavlovic | Towards Data Science.” Accessed: Jan. 25, 2024. [Online]. Available: https://towardsdatascience.com/log-normal-distribution-a-simple-explanation-7605864fb67c

[57] M. Taboga, *“Log-normal distribution”, Lectures on probability theory and mathematical statistics*. Kindle Direct Publishing, 2021. Accessed: Jan. 25, 2024. [Online]. Available: https://www.statlect.com/probability-distributions/log-normal-distribution

[58] P. A. Hassan, S. Rana, and G. Verma, “Making sense of Brownian motion: Colloid characterization by dynamic light scattering,” *Langmuir*, vol. 31, no. 1, pp. 3–12, Jan. 2015, doi: 10.1021/LA501789Z/ASSET/IMAGES/LARGE/LA-2014-01789Z_0004.JPEG.

[59] J. Stetefeld, S. A. Mckenna, and T. R. Patel, “Dynamic light scattering: a practical guide and applications in biomedical sciences,” *Biophys Rev*, doi: 10.1007/s12551-016-0218-6.

[60] A. Einstein and R. Fürth, *Investigations on the theory of Brownian movement*. New York, N.Y.: Dover Publications, 1956.

[61] A. Aitken and M. Learmonth, “Protein Determination by UV Absorption,” pp. 3–6, 1996, doi: 10.1007/978-1-60327-259-9_1.

[62] “Beer–Lambert law,” *The IUPAC Compendium of Chemical Terminology*, Sep. 2008, doi: 10.1351/GOLDBOOK.B00626.

[63] “A Classical Least Squares Method for Quantitative Spectral Analysis with Python | by Nicolas Coca, PhD | Towards Data Science.” Accessed: Sep. 07, 2023. [Online]. Available:

https://towardsdatascience.com/classical-least-squares-method-for-quantitative-spectral-analysis-with-python-1926473a802c

[64] D. C. Harris and C. A. Lucy, *Quantitative Chemical Analysis*, 9th ed. New York, NY: W. H. Freeman and Company, 2016.

[65] M. Pourbaix, “Atlas of Electrochemical Equilibria in-Aqueous Solutions.”

[66] A. Sanchez-Hachair and A. Hofmann, “Hexavalent chromium quantification in solution: Comparing direct UV–visible spectrometry with 1,5-diphenylcarbazide colorimetry,” *Comptes Rendus Chimie*, vol. 21, no. 9, pp. 890–896, Sep. 2018, doi: 10.1016/J.CRCI.2018.05.002.

[67] “ICSC 1531 - CHROMIUM(III) OXIDE.” Accessed: Jan. 18, 2024. [Online]. Available: https://www.ilo.org/dyn/icsc/showcard.display?p_version=2&p_card_id=1531

[68] R. A. Latour, “The Langmuir isotherm: A commonly applied but misleading approach for the analysis of protein adsorption behavior,” 2014, doi: 10.1002/jbm.a.35235.

[69] S. Marchesseau, J. C. Mani, P. Martineau, F. Roquet, J. L. Cuq, and M. Pugnière, “Casein interactions studied by the surface plasmon resonance technique,” *J Dairy Sci*, vol. 85, no. 11, pp. 2711–2721, 2002, doi: 10.3168/jds.S0022-0302(02)74358-0.

[70] H. P. Erickson, “Size and Shape of Protein Molecules at the Nanometer Level Determined by Sedimentation, Gel Filtration, and Electron Microscopy,” *Biol Proced Online*, vol. 11, no. 1, p. 32, 2009, doi: 10.1007/S12575-009-9008-X.

[71] P. A. Fritz *et al.*, “Electrode Surface Potential-Driven Protein Adsorption and Desorption through Modulation of Electrostatic, van der Waals, and Hydration Interactions,” *Langmuir*, vol. 37, no. 21, pp. 6549–6555, Jun. 2021, doi: 10.1021/acs.langmuir.1c00828.

[72] S. Lin, R. Blanco, and B. L. Karger, “Adsorption-desorption isotherm hysteresis of beta-lactoglobulin A with a weakly hydrophobic surface,” *J Chromatogr*, vol. 557, no. 1–2, pp. 369–382, Sep. 1991, doi: 10.1016/S0021-9673(01)87145-4.

[73] T. Hagiwara, T. Sakiyama, and H. Watanabe, “Molecular Simulation of Bovine-Lactoglobulin Adsorbed onto a Positively Charged Solid Surface”, doi: 10.1021/la8024149.

[74] A. A. Thyparambil, Y. Wei, and R. A. Latour, “Experimental characterization of adsorbed protein orientation, conformation, and bioactivity,” 2014, doi: 10.1116/1.4906485.

[75] “Foutenleer Practicum Meten en Maken,” 1986.

Appendix I

Data processing LUMiSizer data

Based on the relation between particle size and sedimentation velocity explained in Chapter 2.3.b. We have written Python code that is able to transform raw LUMiSizer data to custom sedimentation plots and particle size distributions. The found particle size distributions are plotted on log-normal distribution in Excel. Some parts are condensed for readability.

Summary

Time resolved transmission data along the LUMiSizer cuvette is transformed optical density and presented in a more comprehensible manner. On the basis of sedimentation plot the sedimentation velocity of fractions of optical density are determined. We find a range of sedimentation velocities. The error for these velocities is determined. By taking the derivative of the change of the sedimentation velocity and plotting it against the sedimentation velocity we find a distribution. The sedimentation velocity is converted to a particle radius by assuming only stokes drag and the centrifugal force work on the particle. These distributions are then exported to excel for further analysis.

Python implementation

The LUMiSizer produces time resolved transmission plots with the included STEP software, shown in Figure 22. Information about the particle size and the size distribution is present in this graph. Custom Python is used to transform these graphs into for us a more usable form.

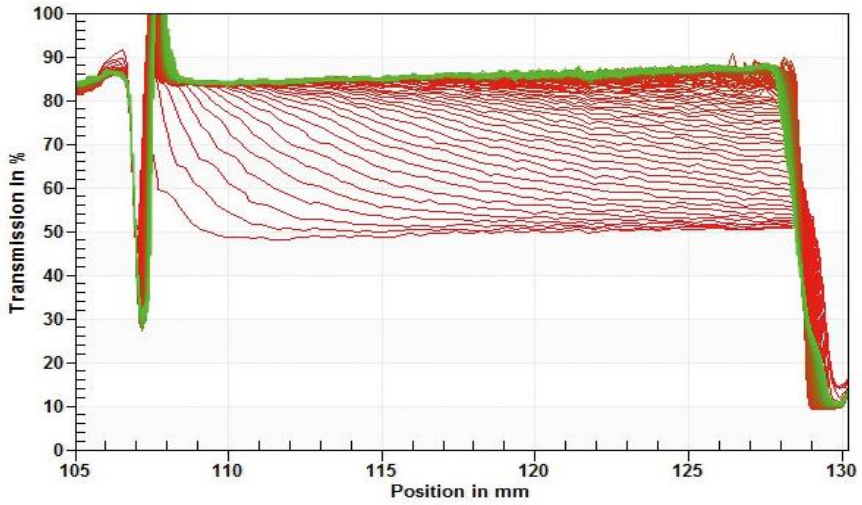

Figure 22 Time resolved transmission plot. The transmission is shown on the y-axis and the position in the cuvette on the x-axis. Every line is one moment in time and the green lines are the last transmissions to be measured.

The raw LUMiSizer data is available in .txt files. To facilitate the data processing in Python the data is first saved as .CSV files. The transmission values are stored in columns with the time as the header and the rows are the position in the cuvette in mm.

For the analysis in Python, we start by importing the required packages:

```
import csv
import numpy as np
from numpy import gradient
import matplotlib.pyplot as plt
import pandas as pd
import math
import os.path
```

The final step in the data processing is the transformation of sedimentation velocity to a hydrodynamic radius. We define the necessary constants here:

```
# Constants
n = 0.0010016 * 1.2 # (pa*s) viscosity water with ~1 wt protein at 20 C
pCr = 4220 # kg/m^3 buoyant mass Cr2O3
rpm = 400 # rpm lumisizer
pi = math.pi
w = rpm /60*pi*2 # rad/s omega
w2r = w**2 * 0.1293 # radius is the radius of the Lumisizer
```

The files as .csv file are loaded into Python. This includes reference files used to determine absorbance form transmission data. File paths for the storage of plots is also defined and lists are defined.

```
file_path = 'U:\My Documents\Python\csv files'
file_path2 = 'U:\My Documents\Python\\figuresSFIT'
file_path_refW = 'U:\My Documents\Python\csv files\water ref pH7.csv'
file_path_refB = 'U:\My Documents\Python\csv files\Black paper ref 255.csv'

# 'U:/Documents/Python/'     # directory with the measured file
input_file_name = "Cr2O3 w 0.25wt% Bipro"   # LUMiSizer exported txt file
input_file_name_incl_path = os.path.join(file_path, input_file_name + ".csv")

output_lum_derivative_plot_jpg = os.path.join(file_path2, input_file_name +
"_lum_derivative_plot.jpg")

number_of_profiles = 255 # total number of profiles
final_time = 0 # starts of counter for time
skipping_nr = 1 # determines how much of the data is used. if 1 all dat is
used, if 2 half is skipped.
v_list = []
r_list = []
v_error = []
dvdz_list = []
z_min_list = []
z_min = 0
```

The particle size distribution is found by examining the distribution of sedimentation velocities. First the sedimentation velocities are calculated from the LUMiSizer data. This is done by calculating the velocity for a fraction of the absorbance values and looping the code till all relevant absorbance values have been examined. We define the loop as follows:

```
while True:
    z_min = z_min + 0.02
    # + number determines step size of the calculation
    z_max = z_min + 0.05
    # + number defines area over which points are taken for a

    def absorbance_plot():…

    absorbance_plot()
    if z_max > 1.1:
        break
```

Where `z_min` the is lower limit of the absorbance and `z_max` the upper limit of the absorbance for the selected fraction. The `z_min = z_min + 0.02` determines the step size between fractions and `z_max = z_min + 0.05` determines the size of the fraction. The loop ends when the max adsorption is larger than 1.1.

For the absorbance plot we first define the area on which the sedimentation velocity is calculated. As described in Chapter 2.3.b we use the sedimentation velocity to calculate the hydrodynamic radius. For this calculation the assumption is made that only the Stokes' drag, and centrifugal force are relevant. This assumption breaks down if the dispersions is too dense. Selection border is chosen to account for this. Here we define these selection borders:

```
def absorbance_plot():

# lists are defined
x_list = []
y_list = []
z_list = []
x_list_fit = []
y_list_fit = []

# selection borders for measuring time, position, and absorption.
# the slope should be between the y_min and y_max, this depends on how far the
tube was filled and the speed
# of sedimentation

x_min = 0
x_max = 2500
y_min = 118
y_max = 125
fit_n = 0
sum_x = 0
sum_y = 0
sum_xy = 0
```

```
sum_x2 = 0
sum_d2 = 0
```

Next the transmission from reference measurements is determined. To transform the measured transmission of the sample to absorbance or more strictly speaking optical density the transmission must be scaled. The transmission of pure water is defined as a 100% transmission and the transmission of cuvette filled with a cut-to-size black piece of paper is defined as 0% transmission. The absorbance is then calculated with:

$$A = -log\left(\frac{T_{sample} - T_{paper}}{T_{water} - T_{paper}}\right) \quad (40)$$

Where the T_{sample} are the transmission values of the sample. T_{paper} is the transmission 0% transmission. T_{water} is the transmission of pure water. The .csv files are loaded in, and the first 10 lines are skipped as they contain information on the SOP. The transmission values are read out for all profiles and saved.

```
counter = 0 # this loads in the 100% transmission, pure water, reference
with open(file_path_refW) as f:
    reader = csv.reader(f, delimiter=";")
    i = 0
    for i in range(1, 11): # this skips the first ten rows
        next(reader)
        i = i +1
    div_ten = skipping_nr - 1

    for row in reader:
        div_ten = div_ten + 1
        if div_ten == skipping_nr:
            counter = counter + 1
            profile_nr = 0
            while profile_nr < number_of_profiles:
                profile_nr = profile_nr + 1
                transmission_water = float(row[profile_nr])

counter = 0 # this loads in the 0% transmission, black paper, reference
with open(file_path_refB) as f:
    reader = csv.reader(f, delimiter=";")
    i = 0
    for i in range(1, 11):
        next(reader)
        i = i + 1
    div_ten = skipping_nr - 1

    for row in reader:
        div_ten = div_ten + 1
        if div_ten == skipping_nr:
            counter = counter + 1  # counter = 0 at position 103.6893; counter
= 1871 bij position 130.0096
            profile_nr = 0
            while profile_nr < number_of_profiles:
                profile_nr = profile_nr + 1
                transmission_paper = float(row[profile_nr])
```

The sample data is now loaded in. With Eq. (40) the transmission values are converted to absorbance values:

```
# first counter loads a v and b value so that the second counter can make an
error calculation
counter = 0
with open(input_file_name_incl_path) as f:
    reader = csv.reader(f, delimiter=";")
    i = 0
    for i in range(1, 11):
        next(reader)
        i = i + 1
    div_ten = skipping_nr-1    # slechts 1 op de 10 punten bewaren, zodat de
berekening sneller gaat
    for row in reader:
        div_ten = div_ten+1
        if div_ten == skipping_nr:
            position = float(row[0])
            y = position
            counter = counter+1     # counter = 0 at position 103.6893;
counter = 1871 at position 130.0096
            profile_nr = 0

            while profile_nr < number_of_profiles:
                profile_nr = profile_nr+1
                x = profile_nr*final_time/number_of_profiles
                transmission = float(row[profile_nr])
                absorbance = -math.log10((transmission - transmission_paper) /
(transmission_water - transmission_paper))
                z = absorbance
```

The absorbance is saved as z, this value is tied to a specific x and y coordinate. In order to generate an absorbance plot the values are added to a list and plotted with a scatter plot. The z values are plotted with a colormap:

```
                x_list.append(x)
                y_list.append(y)
                z_list.append(z)

plt.scatter(x_list, y_list, s=10, c=z_list, vmin=0, vmax=1.3,
cmap='Spectral_r')
plt.title(input_file_name)
plt.xlabel("time (s)")
plt.xlim(0, final_time)
plt.ylabel("radial position (mm)")
plt.ylim(130, 105)
cbar = plt.colorbar(label="Absorbance", orientation="vertical", shrink=0.75)

plt.savefig(output_lum_absorbance_plot_jpg)
plt.show()
```

This generates absorbance plot as shown in Figure 23. The sedimentation of a sample can be interpreted in a more intuitive manner compared to original LUMiSizer plots. The sharp difference between the area with high absorbance and low absorbance is the sedimentation front.

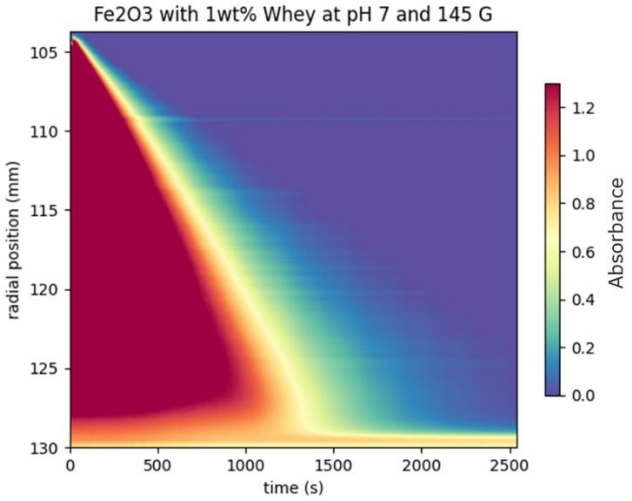

Figure 23 Absorbance plot generated with Python code. The y-axis is the position in the cuvette. The x-axis is the time and the absorbance is represented with a colormap. When the absorbance is high, there are still many particles present at the point and time in the cuvette.

For further data analysis sedimentation velocities are derived from the presented plot. The velocity is the slope of a fraction absorbance values. In Figure 23 a distinct fraction is depicted as a noticeable yellow line, with an absorbance value of 0.6. The slope of the yellow line is the velocity of that fraction.

For the determination of the sedimentation velocities per absorbance fraction the Python script continues at `z = absorbance`. If the data falls within earlier determined selection criteria it is added to a list.

```
        # if values meet criteria below, they are added to a list and the
slope of the plot through these points is determined
        if x_min < x < x_max:
            if y_min < y < y_max and z_min < z < z_max:
                x_list_fit.append(x)
                y_list_fit.append(y)
                fit_n = fit_n+1
                sum_x = sum_x+x
                sum_y = sum_y+y
                sum_xy = sum_xy + x * y
                sum_x2 = sum_x2 + x * x

        x_list.append(x)
        y_list.append(y)
        z_list.append(z)
div_ten = 0

v = ((fit_n * sum_xy) - (sum_x * sum_y)) / ((fit_n * sum_x2) - (sum_x *
sum_x))
b = ((sum_x2 * sum_y) - (sum_x * sum_xy)) / ((fit_n * sum_x2) - (sum_x *
sum_x))
```

where `v` is the sedimentation velocity and b the intercept with y-axis. We use here a first order least-squares method to determine the slope based on the plotted points [75].

The error of the sedimentation velocity and y-intercept is calculated by repeating the calculation and calculate the difference from every fitted point. The calculation is repeated in the loop and altered from the line: `if y_min < y < y_max and z_min < z < z_max:` as shown below:

```
   ……..

                        if y_min < y < y_max and z_min < z < z_max:

                            sum_d2 = sum_d2 + (y-v * x - b) ** 2

        div_ten = 0

sum_d2 = sum_d2 / (fit_n - 2)
s_v = math.sqrt((sum_d2 * fit_n)/((fit_n * sum_x2) - (sum_x * sum_x)))
# error bars for a (sedimentation speed in mm/s)
s_b = math.sqrt((sum_d2 * sum_x2)/((fit_n * sum_x2) - (sum_x * sum_x)))

v = ((fit_n*sum_xy)-(sum_x*sum_y))/((fit_n*sum_x2)-(sum_x*sum_x))
b = ((sum_x2*sum_y)-(sum_x*sum_xy))/((fit_n*sum_x2)-(sum_x*sum_x))

v_error.append(s_v)
v_list.append(v)
```

The velocity is converted to a hydrodynamic radius with Eq. (17) from Chapter 2.3.b.

```
r = (math.sqrt(((9 / 2) * ((n * (v / 1000)) / (pCr * w2r)))) * 1e9)
r_list.append(r)
z_min_list.append(z_min+0.05)
```

The loop is stops when `z_max > 1.1` . The distribution is then determined by taking the derivative of the velocities.

```
print('r_list =', r_list)

dv = gradient(v_list)
dz = gradient(z_list)
dzdv = dz/dv

print('dz/dv =', dzdv)

plt.plot(r_list, dzdv)
plt.title(input_file_name)
plt.xlabel("Radius (nm)")
plt.ylabel("dv")
```

```
plt.savefig(f'U:\My Documents\Python\\figuresSFIT\\{input_file_name}
output_lum_derivative_plot.png')
plt.show()
```

The list with the calculated radii and the probability density (dz/dv) are exported to excel and analyzed further as described in Chapter 2.3.b. in Excel.

Appendix II

Data processing UV-Vis spectroscopy

The theory behind separating absorption spectra is explained in Chapter 2.3.d. Here the implementation of this theory with Python code is shown. Some parts are condensed for readability. For more information the blog post of Nicolas Coca on quantitative spectral analysis is recommended [63].

Summary

Reference spectra of proteins and Cr(VI) are loaded into Python with known concentrations. A horizontal baseline component is loaded in and the sample spectrum is loaded in. All spectra are adjusted to have the same wavelength range and formatting. Reference spectra and baseline are used to generate a spectrum. With NNLS (non-negative least squares) the calculated spectrum is fitted on the sample spectrum by varying the concentrations of the reference spectra. The NNLS opposed to CLS does not allow negative components. Both the fitted calculated spectrum and the sample spectrum are plotted to visually inspect the fit. If fit is satisfactory, concentrations of the components are taken as the concentration of the components in the sample.

Python implementation

We start by loading the necessary Python packages:

```
import numpy as np
import matplotlib.pyplot as plt
import pandas as pd
from numpy.linalg import inv
import os
import scipy.optimize as opt
```

For ease-of-use toggles switching between NaCas and whey protein are implemented. A toggle for the correction of the formatting of the reference spectra is used as well:

```
# Create a toggle to switch between components C and D. now the switch between
protein ref 1 and 2 is manual
use_component_C = False  # Set to True to use component C (Bipro), False to
use component D (NaCas)

# turn one if the sample of interest and protein reference have increasing
wavelength
use_increasing_wavelength_order = False
```

The quality of the fit was improved by limiting the area of interest to between 250 and 500 nm. Below 250 nm the absorption became too strong, and no peaks of interest are above 500 nm. Sample file is loaded in and formatting and selection of `x_range` is applied:

```
# X-axis (Wavelengths)
# the range of the calculated is defined here, (end, start, number of points
```

```
between)
x_range = np.linspace(500, 250, 251)  # Define your desired x_range
# Define the desired wavelength range with 2 nm intervals
new_wavelength_range = np.linspace(500, 250, len(x_range))  # Ensure same
length as x_range
new_wavelength_range = new_wavelength_range[::-1]  # Make sure it's in
decreasing order
# Modify your code to filter out redundant data points


csv_file_path = 'U:\My Documents\Python\csv files\sample.csv'

dataS = pd.read_csv(csv_file_path, delimiter=';', decimal=',')
sample_spectrum = dataS.iloc[:, 1].values
wavelength_range = dataS.iloc[:, 0].values

if use_increasing_wavelength_order:
    sample_spectrum = sample_spectrum[::-1]
    wavelength_range = wavelength_range[::-1]

# Extract the file name from the path
file_name = os.path.splitext(os.path.basename(csv_file_path))[0]

# Create a mask to select data points that match the x_range wavelengths
mask = np.isin(wavelength_range, x_range)

adjusted_sample_spectrum = sample_spectrum[mask]
```

The non-negative least squares formula used to find the concentration of the reference components in the sample spectrum is then defined:

```
def least_sq(adjusted_sample_spectrum, components):

    # adjusted_sample_spectrum: array of x-values, these are in nm.
    # components (reference spectra): array of n (number of components)
columns with x-values.

    # This def returns an array of n values. Each value is the similarity
score for the sample_spectrum and a component spectrum.

    similarity = np.dot(inv(np.dot(components, components.T)),
np.dot(components, adjusted_sample_spectrum))

    nnls_result, _ = opt.nnls(components.T, adjusted_sample_spectrum)

    print('Similarity scores:', similarity)
    print("nnls_result:", nnls_result)

    return nnls_result

# similarity is the fit
```

Next the reference components are loaded in. The reference components are carefully made so that the concentration can be used to solve the sample spectrum. We create in total 5 components. For Cr(VI), component A and B are created; component A is the measured at pH 2 so that the only present absorbing species is $HCr_2O_4^-$, component B is the measured at pH 12 so that the only present absorbing species is $Cr_2O_4^{2-}$.

```
# Component A, pH 2.00 K2Cr2O7
dataA = pd.read_csv('U:\My Documents\Python\csv files\\0.15 mM K2Cr2O7 pH 2.00
reference.csv', delimiter=';')
absorbanceA = dataA.iloc[:, 1].values  # Extracts absorbance column
wavelength_rangeA = dataA.iloc[:, 0].values
# Create a mask to select data points that match the x_range wavelengths
maskA = np.isin(wavelength_rangeA, x_range)

# component B, ph 11.98 K2Cr2O7
dataB = pd.read_csv('U:\My Documents\Python\csv files\\0.15 mM K2Cr2O7 pH
11.98 reference.csv', delimiter=';')
absorbanceB = dataB.iloc[:, 1].values
wavelength_rangeB = dataB.iloc[:, 0].values
# Create a mask to select data points that match the x_range wavelengths
maskB = np.isin(wavelength_rangeB, x_range)
```

For the protein reference components are created. For each batch the stock is carefully diluted and used only as a reference spectrum for that batch. We assume that the protein absorption spectrum is pH independent. For the construction of the calculated spectrum either component C or component D is used depending on the toggle.

```
# component C, whey protein reference
dataC = pd.read_csv('U:\My Documents\Python\csv files\samples 2023926\\Stock 1
0.2 wt Bipro.Sample.Raw.csv', delimiter=';',decimal=',')
absorbanceC = dataC.iloc[:, 1].values
wavelength_rangeC = dataC.iloc[:, 0].values

if use_increasing_wavelength_order:
    absorbanceC = absorbanceC[::-1]
    wavelength_rangeC = wavelength_rangeC[::-1]

# Create a mask to select data points that match the x_range wavelengths
maskC = np.isin(wavelength_rangeC, x_range)

# component D, NaCas reference
dataD = pd.read_csv('U:\My Documents\Python\csv files\samples 20231013\Stock 3
NaCas 0,2 wt.Sample.Raw.csv', delimiter=';',decimal=',')
absorbanceD = dataD.iloc[:, 1].values
wavelength_rangeD = dataD.iloc[:, 0].values

if use_increasing_wavelength_order:
    absorbanceD = absorbanceD[::-1]
    wavelength_rangeD = wavelength_rangeD[::-1]

# Create a mask to select data points that match the x_range wavelengths
maskD = np.isin(wavelength_rangeD, x_range)
```

The last component is a baseline adjustment. To account for a baseline, we found that a horizontal baseline gave a more than adequate fit. A more sophisticated baseline adjustment could be implemented but time limitations prevented further code optimization. The component made by constructing a spectrum with constant absorption at all wavelengths in Excel.

```
# Component Horizontal baseline
dataH = pd.read_csv('U:\My Documents\Python\csv files\\reference component
horizontal .csv', delimiter=';',decimal=',')
absorbanceH = dataH.iloc[:, 1].values
wavelength_rangeH = dataH.iloc[:, 0].values

# Create a mask to select data points that match the x_range wavelengths
maskH = np.isin(wavelength_rangeH, x_range)
```

These four spectra will generate our component matrix or K-matrix from Chapter 2.3.b Eq. (30). The spectra are arranged in rows. The concentrations of the reference components are needed to determine K. Concentrations for component C and D are carefully determined by weighing and are from the same stock as the sample that is analyzed. These determine the final concentration that is reported. The concentration given for the horizontal baseline determines the height of the baseline.

```
# Define the concentrations for components A, B, C, D, and H
concentration_A = 0.150  # mM
concentration_B = 0.150  # mM
if use_component_C:
    concentration_P = 0.2009 # wt # component C
    concentration_C = concentration_P
else:
    concentration_P = 0.1996  # wt # component D
    concentration_D = concentration_P

concentration_H = 0.01

# Create a list of component names and concentrations
component_names = ['Component A', 'Component B']
component_concentrations = [concentration_A, concentration_B,concentration_P,
concentration_H]
```

To ensure that all spectra have the same size a mask is applied:

```
adjusted_sample_spectrum = sample_spectrum[mask]

adjusted_absorbanceA = absorbanceA[maskA]
adjusted_absorbanceB = absorbanceB[maskB]
adjusted_absorbanceC = absorbanceC[maskC]
adjusted_absorbanceD = absorbanceD[maskD]
adjusted_absorbanceH = absorbanceH[maskH]
```

The beforementioned toggle determines which protein is used to create an array with all the components. These are the components of our K-matrix and is saved as `components`:

```
# Determine which component to use based on the toggle
if use_component_C:
    componentP = adjusted_absorbanceC
    component_concentrations.append(concentration_C)
    components = np.array([adjusted_absorbanceA, adjusted_absorbanceB,
adjusted_absorbanceC, adjusted_absorbanceH])
    component_label = 'Component C, Bipro reference'
    component_label2 = 'Component C'
else:
    componentP = adjusted_absorbanceD
    component_concentrations.append(concentration_D)
    components = np.array([adjusted_absorbanceA, adjusted_absorbanceB,
adjusted_absorbanceD, adjusted_absorbanceH])
    component_label = 'Component D, NaCas reference'
    component_label2 = 'Component D'
```

The components are individually plotted this is the left plot in Figure 24.

```
plt.figure(figsize=(12, 6))  # Adjust the width and height as needed
plt.subplot(1, 2, 1)  # 1 row, 2 columns, first subplot
plt.plot(x_range, adjusted_absorbanceA, label='Component A, pH 2.00
K$_{2}$Cr$_{2}$O$_{7}$')
plt.plot(x_range, adjusted_absorbanceB, label='Component B, pH 11.98
K$_{2}$Cr$_{2}$O$_{7}$')
plt.plot(x_range, componentP, label=component_label)
plt.plot(x_range, adjusted_absorbanceH, label='baseline correction')
plt.title('Known components in our mixture', fontsize=15)
plt.xlabel('Wavelength (nm)', fontsize=15)
plt.ylabel('Absorbance', fontsize=15)
plt.legend(fontsize=10)
```

The next step is to compare the sample spectrum with the reference components. The non-negative least squares method is then used to recalculate the concentrations of the components to minimize the difference with the sample spectrum.

```
# Apply non negative least squares method
cs = least_sq(adjusted_sample_spectrum, components)
```

This uses the definition for `least_sq` that we gave in the beginning and calculates a spectrum. Both the sample spectrum and the calculated spectrum are then plotted to visually inspect the quality of the fit:

```
plt.subplot(1, 2, 2)  # 1 row, 2 columns, second subplot
```

```
plot_title = 'Mixture spectrum and calculated components'
sample_name2 = 'raw'

plt.plot(x_range, adjusted_sample_spectrum, color='black', label=sample_name)
# Plots the unknown sample spectrum

plt.plot(x_range, np.dot(cs, components), color='red', linewidth =2,
label='Calculation') # Plots the calculated spectrum

for i in np.arange(len(cs)):
    concentration_units = 'mM' if i in [0, 1] else 'wt'  # Use 'mM' for
components A and B, 'wt' for C and D
    legend_label = f'{component_names[i]} = {np.round(cs[i],
4)*component_concentrations[i]:.4f} {concentration_units}' if i in [0,1,2]
else 'baseline correction'
    plt.plot(x_range, cs[i]*components[i], label=legend_label)


plt.title(plot_title, fontsize=15)
plt.xlabel('Wavelength (nm)', fontsize=15)
plt.ylabel('Absorbance', fontsize=15)
plt.legend()
# Adjust subplot spacing
plt.tight_layout()

plt.savefig(f'U:\My Documents\Python\\figures CLS method\samples
20231013\{sample_name} {sample_name2}.png')

plt.show()
```

The resulting plot is shown in Figure 23. The concentrations of the components are reported in the legend. Which is found by multiplying the component concentrations with reported reference component concentration.

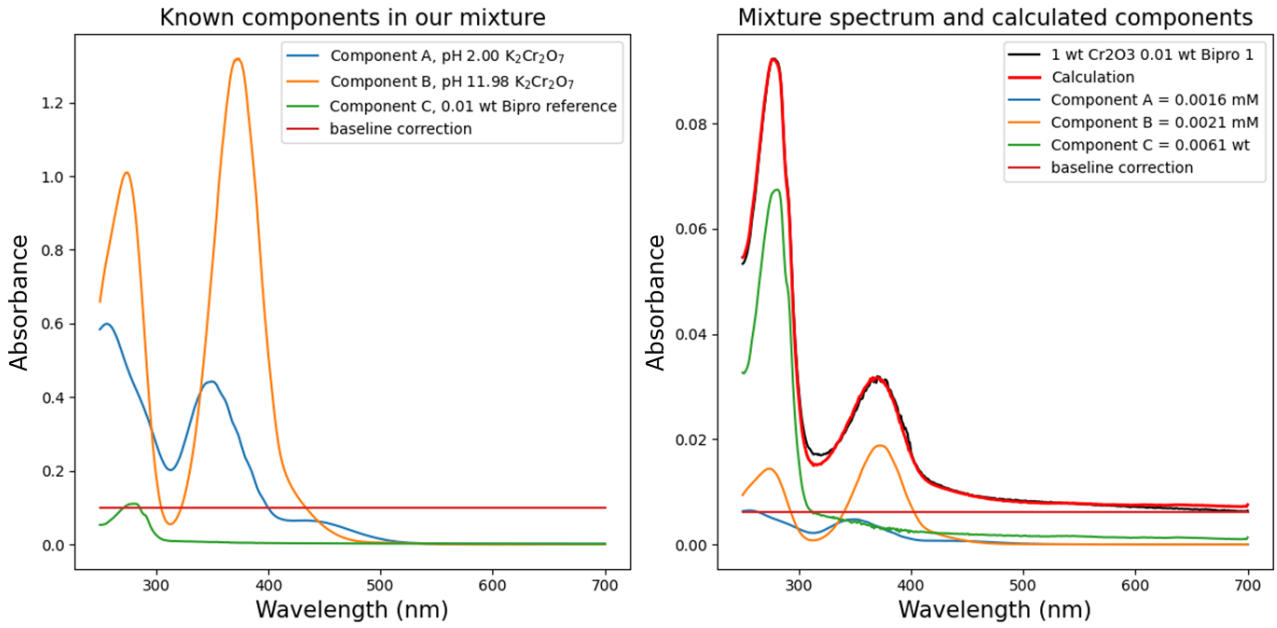

Figure 24 Python plots of a sample spectrum resolved with NNLS method. Left are the reference components. Right are the sample spectrum, calculated spectrum, and the scaled reference components.

The goal of this exercise was to determine the protein concentration in the sample. This is the concentration of the protein component times the reference concentration. This printed with 3 decimals as shown below and processed further in Excel.

```
# this prints the concentration in wt for the protein component, the f'{...,3)}' gives the amount of decimals now 3
print(f'{np.round(cs[2] * component_concentrations[2], 3)}')
```

Appendix III

LUMiSizer PSDs of Cr_2O_3 with whey protein

Particle cluster distribution for Cr_2O_3 (2 wt%) with whey protein (0.5 wt%) between pH 3 and pH 7. Hollow points are not used for the fit of the log-normal distribution. PSDs are volume weighted.

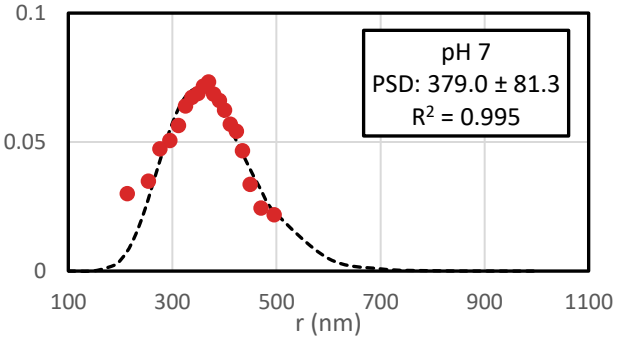

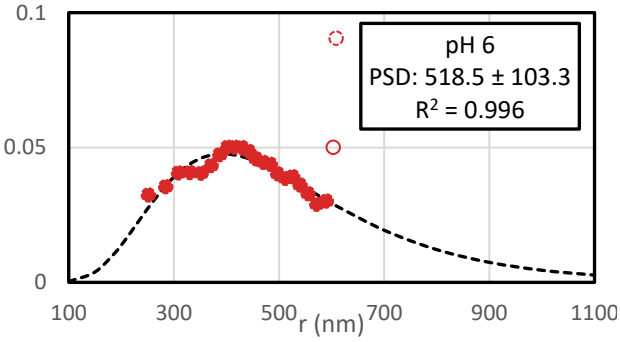

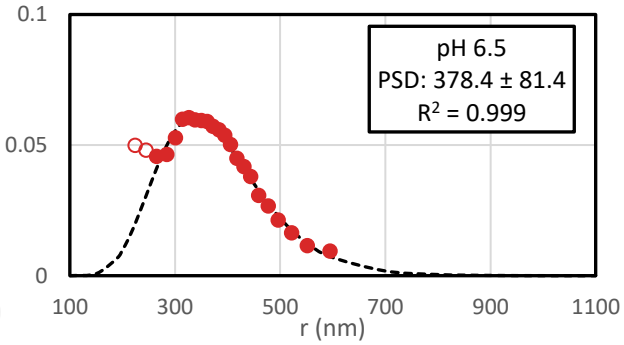

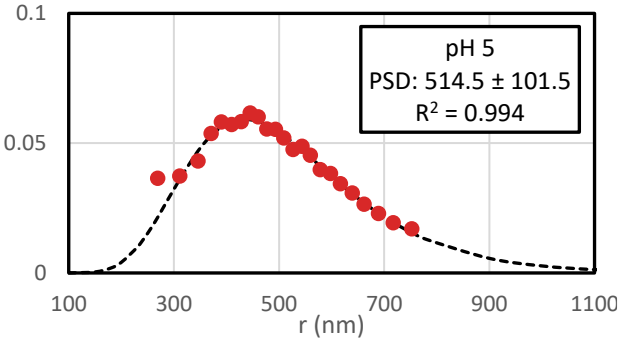

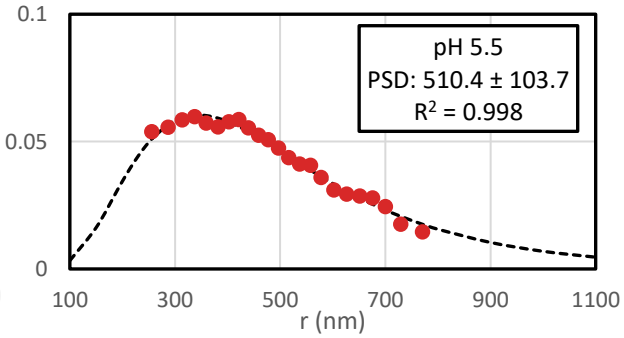

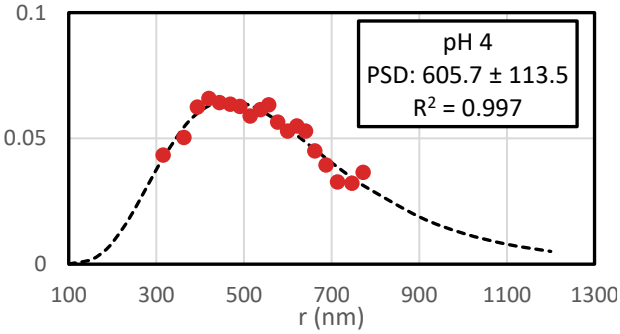

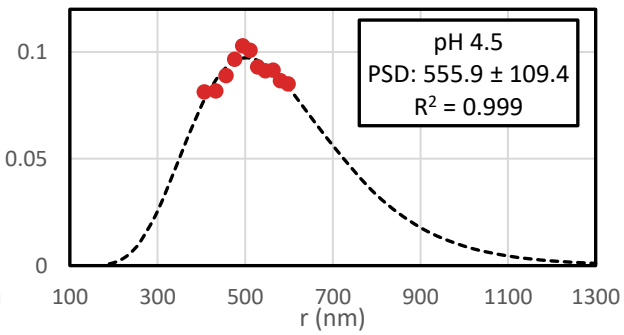

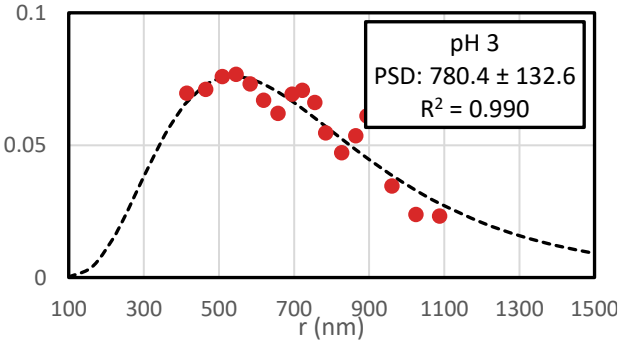

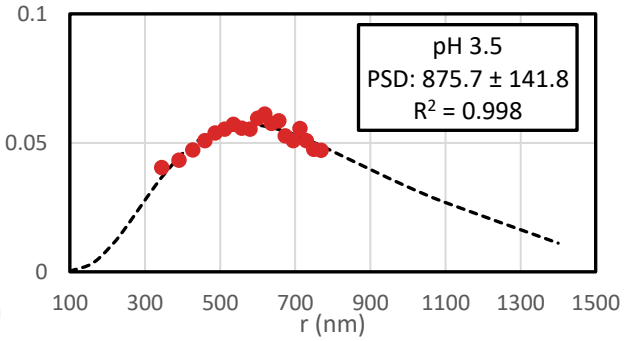

LUMiSizer PSDs for Cr_2O_3 with NaCas

Particle cluster distribution for Cr_2O_3 (2 wt%) with NaCas (0.5 wt%) between pH 3 and pH 7. Hollow points are not used for the fit of the log-normal distribution. PSDs are volume weighted.